REPORT DOCUMENTATION PAGE

Form Approved
OMB NO. 0704-0188

1. AGENCY USE ONLY (Leave Blank)	2. REPORT DATE	3. REPORT TYPE AND DATES COVERED
	July 18, 2002	June 1, 1998 - May 31, 2002

4. TITLE AND SUBTITLE
Computation of Separating High Reynolds Number Incompressible Flows Using Uniform Cartesian Grids

5. FUNDING NUMBERS
DAAG55-98-1-0316

6. AUTHOR(S)

Dr. John Steinhoff, Principal Investigator

7. PERFORMING ORGANIZATION NAME(S) AND ADDRESS(ES)

The University of Tennessee, Space Institute
411 B. H. Goethert Parkway
Tullahoma, TN 37388-9700

8. PERFORMING ORGANIZATION REPORT NUMBER
~~P-38703-EG~~

9. SPONSORING / MONITORING AGENCY NAME(S) AND ADDRESS(ES)

U. S. Army Research Office
P.O. Box 12211
Research Triangle Park, NC 27709-2211

10. SPONSORING / MONITORING AGENCY REPORT NUMBER

38703.8-EG

11. SUPPLEMENTARY NOTES
The views, opinions and/or findings contained in this report are those of the author(s) and should not be construed as an official Department of the Army position, policy or decision, unless so designated by other documentation.

12 a. DISTRIBUTION / AVAILABILITY STATEMENT

Approved for public release; distribution unlimited.

12 b. DISTRIBUTION CODE

13. ABSTRACT (Maximum 200 words)

See Attached Report

14. SUBJECT TERMS

15. NUMBER OF PAGES
81

16. PRICE CODE

17. SECURITY CLASSIFICATION OR REPORT	18. SECURITY CLASSIFICATION ON THIS PAGE	19. SECURITY CLASSIFICATION OF ABSTRACT	20. LIMITATION OF ABSTRACT
UNCLASSIFIED	UNCLASSIFIED	UNCLASSIFIED	UL

NSN 7540-01-280-5500

Standard Form 298 (Rev.2-89)
Prescribed by ANSI Std. 239-18

Computation of Separating High Reynolds Number Incompressible Flows Using Uniform Cartesian Grids

ARO Contract DAAG55-98-1-0316

Final Report

Submitted by:

John Steinhoff

Principal Investigator

The University of Tennessee Space Institute

Submitted to:

Dr. Tom Doligalski

Army Research Office

July 18, 2002

I. Introduction

Most of the research done during the contract period is reported in the "Interim Report" of March, 2002. This is included in section II. Other results, including a breakthrough that has lead to a new, simpler, fully conservative Vorticity Confinement formulation will be discussed in section III. Results of the original formulation for blunt body flow, including comparisons with experiment, are described in section IV. A new, more effective way to treat the surface boundary layer that can be compared with other Vorticity Confinement separation results, such as dynamic stall, is presented in section V. A few of the publications produced during the contract period, which contain relevant material refered to in this report, are included as appendices.

II. Interim Report, March 25, 2002

II.1 Introduction to Interim Report

Thin, fixed or deformable lifting surfaces are very important components of many Army aerodynamic vehicles and devices. These include rotorcraft blades, tail fins, lifting devices attached to them such as leading edge and trailing edge flaps and landing devices such as parachutes, to name a few. It is well known that the development and incorporation of any aerodynamic technology such as described above requires a large number of accurate simulations to be performed. Due to the high Reynolds number, complex geometry and aeroelastic effects, wind tunnel testing is very expensive, for these cases limited to only a small number of tests, and in some cases, not feasible in current facilities at full scale. Hence, it is necessary that computational simulations be done. These must be efficient, requiring short set-up and computing times if they are to be effective in the engineering design process. Unfortunately, conventional computational methods fall far short of this requirement for these flows: Conventional grid-based Euler or viscous ("Navier Stokes") turbulent modeling methods require surface fitted or adaptive grids which often must be very fine near the surface, and require far too much computing and set-up time to be useful for routine engineering/design applications. This problem is even more serious when the surface is deforming so that grid must be continually regenerated. Further, conventional grid based methods also cannot feasibly be used when convecting vortical effects are important because of numerical dissipation. Finally, integral methods such as panel methods, while being efficient, cannot treat general separating cases with associated vortical effects.

Over the past several years we have developed a method that alleviates all of the above problems, *but for blunt body flows* [1–6]. This method allows the rapid, simple treatment of complex geometries, including modeling of the relevant effects of turbulent boundary layers, and general separation, as well as the computation of convecting, thin vortical regions, with no numerical diffusion. The method is based on our Vorticity Confinement computational technique. It utilizes uniform Cartesian grids with "immersed boundaries" for the blunt body surfaces as well as for the convecting vortices. The basic technique is described in Refs. (1-6).

The reason that this original method is not currently used for thin surfaces is that it requires that there be "ghost" points in the body to extrapolate the external flow variables. This poses no problem for the intended (large class of) blunt body flows where at least several grid points can be included across the body, i.e., the body must be at least several grid cells thick. This method has been validated for a number of cases [1-6] and shown to be accurate for these flows.

Currently, an extension of the method is being implemented which results in more accurate inviscid computations for attached flow regions (second order instead of first) and utilizes a separate boundary layer integral computation on the surfaces. This new extension results in simpler turbulent boundary layer modeling than the original Confinement method, since it utilizes a lower dimensional (surface) grid. For example, in 3-D it can use 2-D surface points, which can be dense, rather than the coarser 3-D flow grid points near the surface. This new technique is described below in Sec. II.2. The current version also uses points inside the body and hence has the same limitation to thick, blunt bodies as the basic, original Vorticity Confinement method. However, since it involves solving boundary layer equations directly on the surface and coupling them to an outer inviscid solution on a fixed, uniform grid, it can be extended to treat thin, embedded surfaces.

II.2 Development of Simple Boundary Layer Model Including Separation Using Surface Coordinates

During the performance of our current ARO contract involving blunt bodies: "Computation of Separating High Reynolds Number Incompressible Flows Using Uniform Cartesian Grids", a new extension was discovered that leads to far more efficient computation of separating flows, with far greater control over the boundary layer dynamics than our original Vorticity Confinement based method. This method is termed "Surface Boundary Layer Model" (SBLM). Further, in addition to Cartesian grids, the new SBLM method can be implemented in existing, conventional inviscid codes which utilize body conforming grids, giving them the ability to model boundary layer effects leading to blunt body separation from smooth surfaces, with essentially no increase in computational requirements.

II.2.1 Rationale for SBLM

The aerodynamic forces on surfaces of blunt bodies are determined, to a large extent, by the zone of separation. This, in turn, depends on the dynamics of the boundary layer (BL), which is turbulent for most flows of interest. The detailed dynamics can be solved, without averaging, by direct Navier Stokes simulation ("DNS"), but only for very small regions of the BL at realistic Reynolds numbers. Thus, for general flows, the detailed dynamics cannot be feasibly computed and must be modeled in terms of some averaged variables. Our general approach is to treat the spatial resolution of the BL in a way that is consistent with the temporal resolution: Since the BL flow variables are treated as averaged over short periods of time, as in typical "Reynolds Averaged Navier Stokes" (RANS) treatments, we maintain that a simple, consistent model should involve flow variables that are *also* averaged over small regions of space. Since the time averaged flow (when attached) is smooth *along* the

surface, the averaging is most important normal to the surface - through the BL. This amounts to using variables that represent BL quantities integrated normally through the BL, such as a (small number of) moments. This is very different from the common RANS approach of trying to solve for the spatial details (in the normal direction) without spatial averaging of some time-averaged profile within the BL, which requires very fine grids which are body conforming. Our treatment is consistent with the dominance of large scale coherent structures in the BL for which the temporal fluctuations are comparable to the spatial, which are, in turn, comparable to the BL thickness[7].

One method for constructing such a crude, averaged BL treatment with a minimal number of variables is to use the original Vorticity Confinement method[1-6]. This results in thin vortical BL regions spread over ~ 2 grid cells normal to the surface, which essentially have only a few degrees of freedom.

II.2.2 Surface Boundary Layer Model (SBLM)

The subject of this proposal is the development of a BL model that can treat thin lifting surfaces less than one grid cell thick. Since our original BL scheme requires grid points inside the boundary (on which velocity is set to zero), this was not possible. The new method, however, is far simpler than the original Vorticity Confinement-based scheme, and much more amenable to analysis and as stated, can be extended to thin surfaces extension. In addition, it does not have the problems of loss of resolution due to the ~ 2 cell BL thickness of the original method which would increase the thickness of a thin surface by up to 4 cells. As a result, since it has no displacement thickness errors, the new method can even treat small features that have essentially zero thickness. In addition, the method can still be used with thick, blunt bodies.

The main idea is to combine a new, simple inviscid immersed boundary treatment with a BL model that "lives" on the surface. The inviscid solution, which is smooth, is developed on the uniform Cartesian grid outside the surface. The pressure from this solution is extrapolated onto the separate surface grid nodes using a special inviscid flow model. Then, a lower dimensional partial differential equation is solved on the surface for the (model) tangential velocities which represent the integral in the normal direction of the time averaged BL velocities. The tangential gradient of the computed surface tangential velocities is then used to compute a normal velocity at the outer edge of the boundary layer, through the continuity equation. In an adverse pressure gradient, the divergence of the tangential gradient of this tangential velocity leads to a sudden increase in normal BL velocity (BL "eruption"), which initiates separation.

Although it may seem that this new method requires additional data (a surface grid) compared to the original Vorticity Confinement-based BL method, which only utilized the uniform Cartesian grid, this is not true: the original surface description in all of our applications involves a set of surface nodes (usually surface triangles), which are used to compute a level set "distance" function on each Cartesian grid node. This function then defines the surface. Thus, this surface grid structure is already required; we are now going to have a second use for it in the new BL method.

The new BL method is explicitly consistent with the scenario that the physical BL is

very thin before separation and does not affect the outer, inviscid flow, as it evolves along the surface, driven by the pressure gradient of the outer flow and surface friction, and that, when it "erupts", it initiates separation in the outer flow.

First, the inviscid solution method will be described, then the surface BL model. It will be seen that not only is the BL modeled, but, for the inviscid solution, the near (sub-grid scale) region just exterior to the surface is also modeled.

II.2.2.1 Near-Surface Inviscid Solution Method

As in our original method, we still discretize and solve the continuity and momentum equations with Vorticity Confinement terms on a uniform Cartesian grid[1-6]. The main difference is that the velocity on the grid nodes near the surface (within one cell) are determined differently: The tangential velocity is determined by Surface Vorticity Confinement, which effectively enforces zero vorticity in the grid cells exterior to the surface region. The inviscid near-surface "model" referred to above then specifies the normal velocity at nodes in the near-region (see Fig. 1).

Even though the BL does not result from a balance of diffusion and confinement, as it did in the original Confinement based method, Vorticity Confinement is still vital here: Numerical errors normally create vorticity which, without Confinement, will diffuse and convect away from the boundary region, contaminating the outer flow field with large errors: Confinement prevents this by convecting erroneous vorticity back into the boundary surface, and results in a well-defined outer inviscid flow.

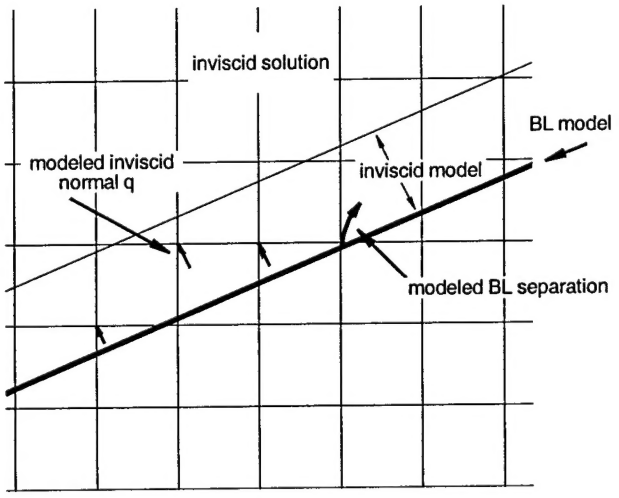

Figure 1: Computational Method

The near-surface inviscid model specifies that $\nabla_s \vec{q}_s$ is independent of normal distance, n, in the near boundary region, where ∇_s is the derivative along the surface (in our initial work, we approximate the surface as a flat plate). This inviscid model is reasonable because the outer vorticity is zero before separation, implying

$$\partial_n \vec{q}_s - \nabla_s q_n = 0$$

where the normal velocity, q_n, is zero on the boundary, and its n derivative varies smoothly along the surface. Thus q_n is $O(h)$ (grid cell size) except at separation. Accordingly, $\partial_n \vec{q}_s$ is $O(h)$ and $\vec{q}_s$ only varies by $O(h)$ in the near surface "inner" modeled region, of thickness h. Then, $\nabla_s \cdot \vec{q}_s$ can be taken to be independent of n to $O(h)$. At a point n above the surface ($n \sim O(h)$), then, we can model q_n by integrating

$$\partial_n q_n = -\nabla_s \cdot \vec{q}_s$$

This gives

$$q_n \approx -n(\nabla_s \cdot \vec{q}_s)|_{n=0} + q_n^b$$

where q_n^b represents the effect of the boundary layer model, and is described in Sec. II.2.2.2. The value of q_n is enforced at nodes just outside the surface (see Fig. 1).

Results of an inviscid computation (without, of course, separation) of a vortex in a straight channel (not aligned with the grid) using the new method are presented in Fig. 2.

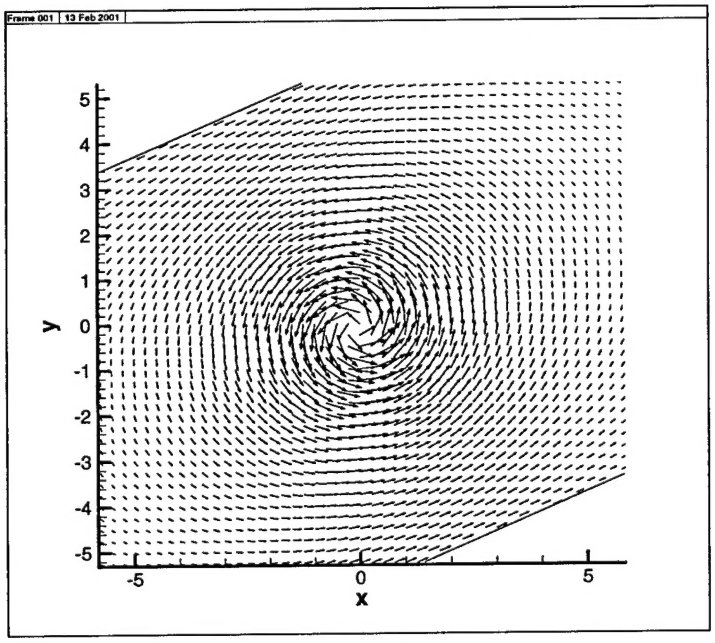

Figure 2: Velocity vector of an inviscid computation of a vortex in a straight channel

There are many opportunities to include effects such as surface curvature here, as well as other near surface inviscid models. For example, for long, thin lifting surfaces, a lifting-line

model for main and tail rotor blades with sub-grid scale chord was recently implemented as a "near surface inviscid model" for a project for United Technology Research Corp.[8]. There, only a uniform Cartesian grid was used which the lifting lines moved through. This project resulted in a code able to predict flow over an entire rotorcraft including fuselage, empennage including tail and, as described, main and tail rotors. Here, the rotor "surface" was a blade with chord assumed so small that it was less than a grid cell and, as a result, the blade could be approximated by a vortex filament with specified motion. (This project really was a preliminary, simplified application of the inviscid part of the model to thin surfaces).

II.2.2.2 Boundary Layer Model

The new BL model is effected directly on nodes on the surface. This model is easy to analyze and modify with additional terms since it exists on a lower dimensional surface and is driven by a pressure field extrapolated from a smooth, exterior inviscid solution. The equations to be solved along the surface are:

$$\partial_t \vec{q}_s^b = -\vec{q}_s^b \cdot \nabla \vec{q}_s^b - \nabla_s (p^e/\rho) + \vec{f}_s \tag{1}$$

where $\vec{q}_s^b$ is the model tangential velocity for the boundary layer: it is single valued at each point and represents a model for the velocity averaged through the layer in the normal direction as well as averaged in time. Also, $\nabla_s(p^e/\rho)$ is the tangential derivative of the inviscid, near surface outer pressure field extrapolated to the surface, divided by the density, ρ. The surface effect, $\vec{f}_s$, can be represented by a number of forms. This is essentially our "turbulent boundary layer model". Without it, there is no separation and the surface velocity equals the near-surface inviscid velocity. A simple, single parameter "drag" model that we are using initially is

$$\vec{f}_s = -\mu \vec{q}_s^b$$

This is one of the simplest possible forms and is an obvious first choice. This model was studied for flow over a 2-D cylinder induced by a pair of convecting vortices as they approached a cylinder[5]. There, it was shown to lead to a singularity in $\nabla_s \vec{q}_s^b$. This is expected since eqn. (1) is just Burger's equation with an imposed forcing function and it is known[9] that, in 1-D,

$$\partial_s q_s^b \longrightarrow -\frac{c}{t_c - t}$$

for t_c, c constants. That is, the gradient diverges at a particular position and time.

The last part of the BL model simulates the effect of incompressibility. It represents, in a simple way, what happens in more detailed computations of a separating boundary layer[10]; when the tangential gradient of the tangential velocity diverges, the gradient of the normal velocity diverges, since incompressibility implies

$$\partial_n q_n^b = -\nabla_s \cdot \vec{q}_s^b$$

Taking $\vec{q}_s^b$ to be a mean velocity through the BL with assumed thickness $\delta \ll h$, with $q_n = 0$ at the surface, this results in

$$q_n^b = -\int_0^\delta \nabla \cdot \vec{q}_s^b dn$$

or

$$q_n^b = -\delta \nabla_s \cdot \vec{q}_s^b$$

This normal velocity is added to the model normal velocity on the outer grid nodes for the inviscid near-boundary solution described above in Sec. II.2.2.1.

During most of the time q_n^b will be small and have little effect, since $\nabla \cdot \vec{q}_s^b$ is $O(1)$ and δ is small. However, when the gradient diverges q_n^b will become large and result in a large q_n^b and, hence, a BL eruption. While the detailed BL computation of Ref. (10) had to be stopped at this point because it did not treat the outer flow, ours can continue. Preliminary results of such an eruption (prescribed q_n^b) have shown that it leads to separating vortices[6].

II.2.3 Current Work

During this final phase of our current ARO project, we are solving vortex-induced separation in 2-D, and 3-D flows over circular cylinder, ellipsoid and sphere, with different grid sizes, in order to calibrate the BL model and determine the best values for the coefficients μ and δ and whether other terms (such as tangential derivatives or surface curvature dependence) are necessary, or whether μ and δ should, themselves, be solutions to a surface-transport equation.

Fig. 3 show the comparison of flow over cylinder with exact solution. Turbulent boundary layer effects can be modeled as shown in Fig. 4. Fig. 5 and Fig. 6 show the velocity vector of the inviscid flow over an ellipsoid and a sphere respectively.

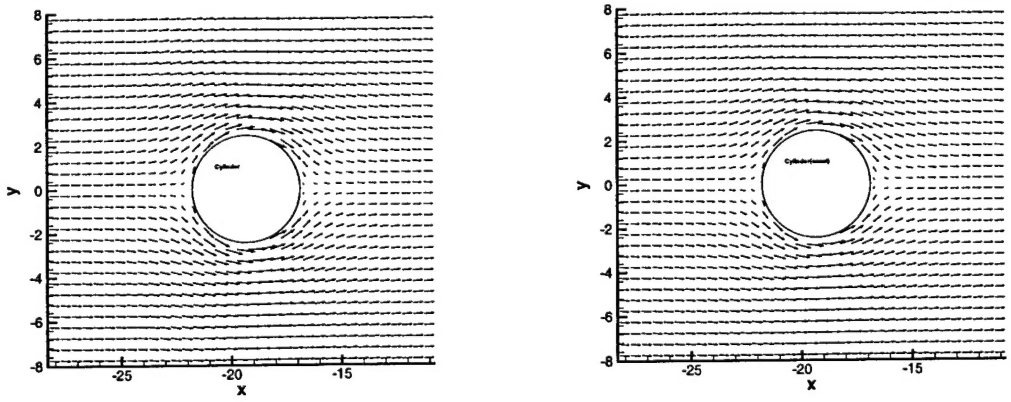

(a) Inviscid cylinder with SBLM

(b) Exact solution

Figure 3: Comparison of Velocity Vector of Flow over Cylinder

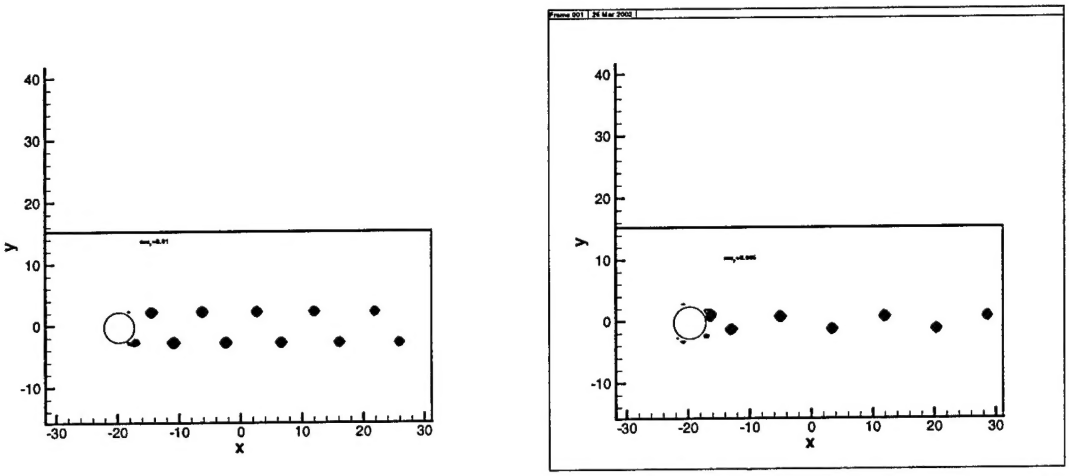

(a) $\mu = 0.01$ (b) $\mu = 0.005$ (with delayed separation)

Figure 4: Vorticity Contour of Vortex Shedding (Model of Turbulent B.L. Effects)

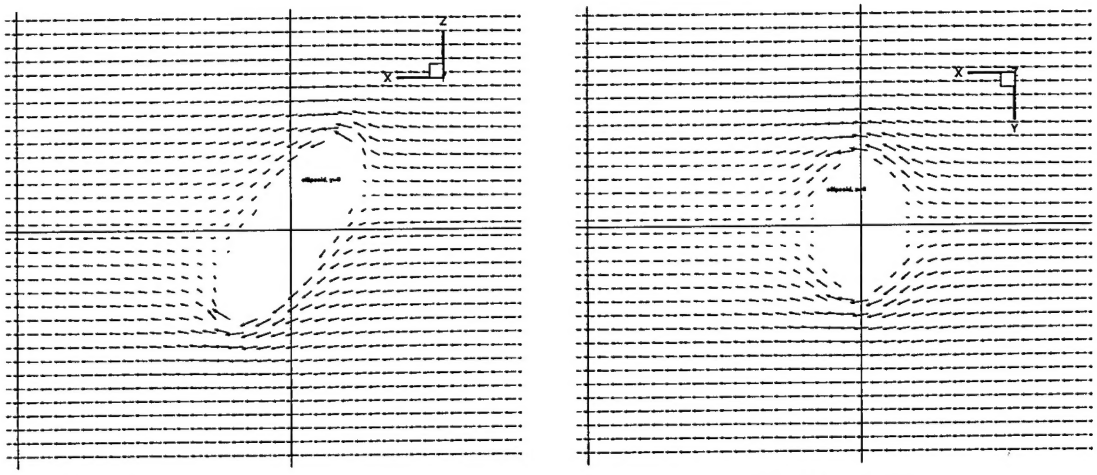

(a) Side View (b) Top View

Figure 5: Velocity Vector of Inviscid Flow over Ellipsoid

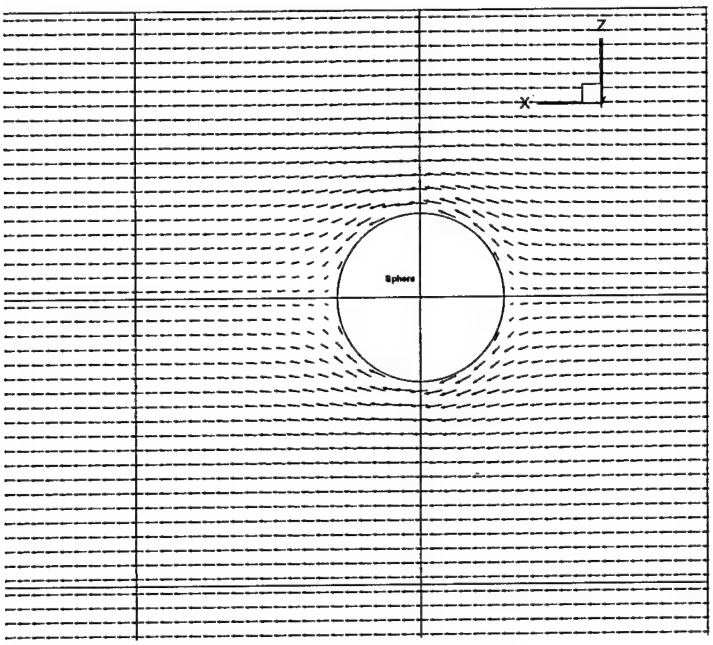

Figure 6: Velocity Vector of Inviscid Flow over Sphere

II.3 Development of Surface Boundary Layer Model for Thin Surfaces

As explained above, computation of flow over general, thin, fixed surfaces is currently not feasible, with conventional methods, for rapid engineering computations: For general, separating flow the very fine body fitted grids necessary for conventional viscous computations cannot be feasibly generated because the surfaces generally are thin and, further, can move in response to aerodynamic or actuator forces, requiring continual re-generation. Further, current pde-based turbulent models are too expensive to routinely run for changing, complex geometries. Our SBLM approach totally alleviates these problems while not requiring any more turbulence modeling parameters than conventional pde-based turbulent modeling schemes. This is because only a regular, coarse inviscid-size Cartesian grid is used together with a separate surface grid, on which a simplified turbulence model is solved, so that the computation is very efficient.

As explained above, a first, simplified example of this approach has already been demonstrated for United Technology Research Corp.[8] using a flexible lifting line model for the rotor blades (both main and tail) together with table look-up, coupled to the main flow field computation. Of course, the blades were not treated as surfaces and no boundary layer model was employed.

A next step, suggested by Frank Caradonna, involved computing inviscid flow over a zero thickness flat plate at different angles of attack in 2-D. Basically, this demonstrates the

accuracy of the coupling of the near surface inviscid model to both the outer flow field and the surface equation solver (see Fig. 1). Here, the surface equations only involved an inviscid pressure computation and integration (to get the lift coefficient). Even though no turbulence model was involved, the resolution requirements of this problem are very demanding since the pressure is singular at the leading edge. Our surface grid approach allows us to resolve this case since the surface grid can be far finer than the (higher dimensional) regular field grid. As in the above lifting line approach, this study was really a preliminary test of the concept of the work proposed here.

Besides demonstrating an important aspect of our approach, this case is extremely important for practical rotorcraft computations: even with fixed, non-deforming surfaces, there are always important lifting surfaces such as tails that cannot be treated as lifting lines since, unlike rotor blades, they have a small aspect ratio. On the other hand, they are too thin for our original Vorticity Confinement treatment, which would require that the outer grid be fine enough to have cells within the thickness of the surface, resulting in fine grids with very large numbers of cells. This was adequate for our original blunt-body based surface treatment but not for the present proposed project, and was the main drive for developing the new, thin-surface method. Further, the assumption of zero thickness here forms a good basis, since effects of finite, small thickness for thin lifting surfaces are usually small and, if needed, are best treated as a perturbation of our simple, efficient method.

The basic idea for the flat plate is to use a closed-form solution in a uniform free stream as a near-surface inviscid model. This is analogous to a Biot Savart model for the lifting line model or the constant tangential velocity and linearly increasing normal velocity model for the infinite flat surface described in Sec. II.2. Thus, the lifting line corresponds to zero chord, the short plate here to finite chord and the flat surface of Sec. II.2 to infinite chord.

Basically, in all of the cases, near the surface the flow is assumed to be the sum of a local uniform free stream (to be determined as part of the coupled computation) and a model term. In all three cases, the main point is to extrapolate the outer velocity into the near-surface region and compute an effective free stream velocity, and then to use this to both get the effect of the surface on the outer flow, and the pressure on the surface. Once this surface pressure is computed, our viscous model which computes separating flow, described in Sec. II.2, can be used.

For the flat plate, an exact, analytic solution[11] was used as the starting point. This is shown in Fig. 7, where V is the (local) free stream velocity magnitude and α the angle between local free stream and the flat plate. The equation shown gives the normal (q_n) and tangential (q_s) velocities at a nearby point, P. During the overall computation, these values are computed at (outer, Cartesian) grid points near the flat plate for cell nodes where the cell intersects the plate. Conventional difference equations, together with Vorticity Confinement are used elsewhere. Matching the solutions determines the local V and θ. This is then used in the equation of Fig. 7 to determine the velocity at points on the surface. The resulting pressure is then computed and integrated to get C_l. For the computations, a 256×256, uniform Cartesian outer grid was used and a 1000 uniform point surface grid. Computed C_p values on the surface for angles of attack (α) of 1°, 5° and 10° are presented in Fig. 8. They are exact since the closed form solution was used and the iterated coupling technique determined the correct local free-stream flow (the local flow near the surface, here denoted

"free stream" is, of course, not input to the model but must be determined since, in general, it is not known but is part of the flow computation). As a final test, the computed surface pressure was numerically integrated to get C_l as a function of α. This is plotted in Fig. 9. It can be seen that it is very close to the theoretical $2\pi\alpha$ line. This agreement is very significant and represents a breakthrough because of the singular nature of the pressure. It should be mentioned that this solution is only meant to be a demonstration of the matching technique. The use of this analytic closed form local 2-D solution, as above, should be useful for long thin rotor blades, including surface effects: It will be a great improvement over lifting line schemes, while being just as fast. The actual analytic form will not be used for short aspect ratio surfaces such as fins. These will be treated by the flat-surface technique described above (for channel flow).

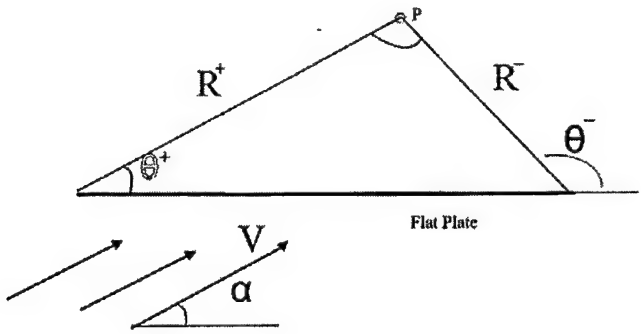

$$\theta = (\theta^- - \theta^+)/2$$

$$R = (R^-/R^+)^{1/2}$$

$$q_s = VR\sin\alpha\sin\theta + V\cos\alpha$$
$$q_n = VR\sin\alpha\cos\theta$$

Figure 7: Velocity Formula for Flat Plate

III. New Vorticity Confinement Formulation

In spring, 2002, we discovered a radically different Vorticity Confinement formulation. This new formulation is completely conservative. The original formulation had (small) effects due to non-conservation: There could be small deviations in the trajectory of vortices. These could be corrected by adding terms to the original formulation to make it fully

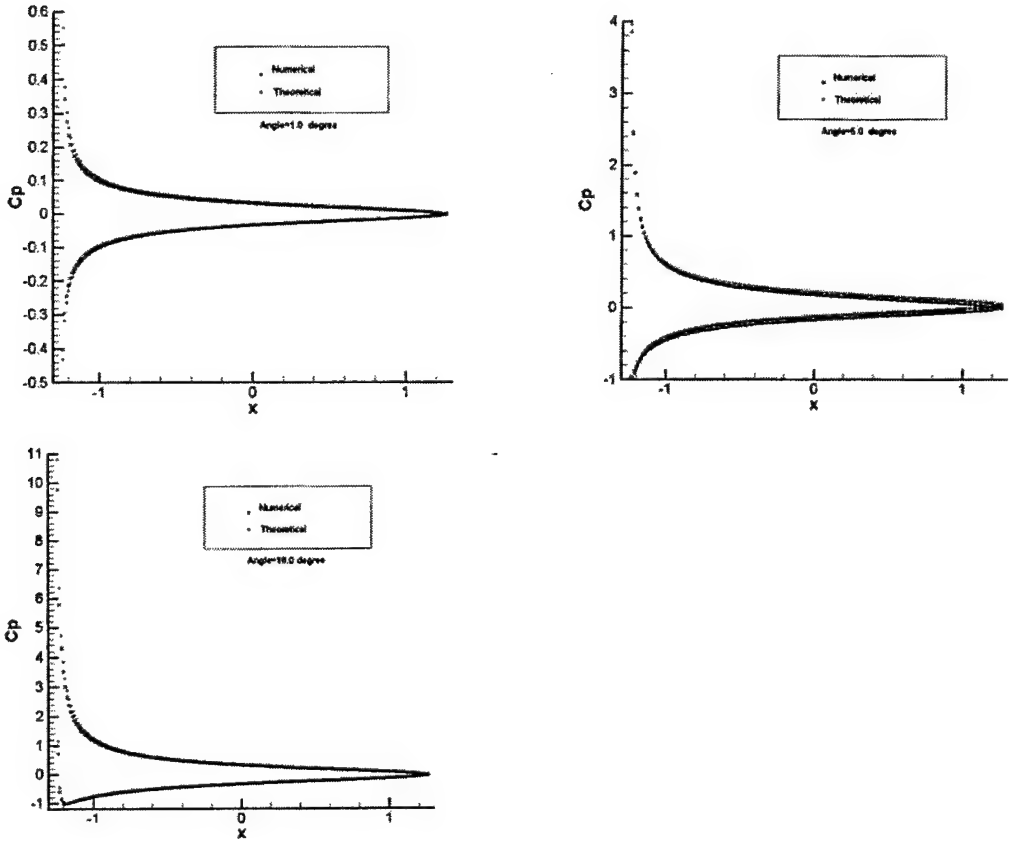

Figure 8: C_p Distribution at Different Angles of Attack

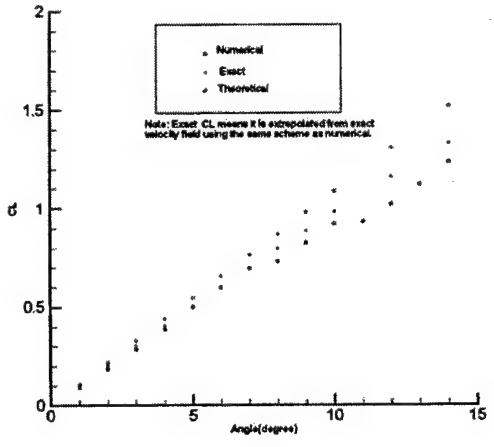

Figure 9: C_l Versus Angle of Attack

conservative[12]; but the result was somewhat complicated. The new form is not only simpler, but is amenable to analysis. It can also be used directly for "scalar confinement", which is important for convection of passive scalars. The reason for the simplicity is that it only involves a simple difference formulation with no extra logic: A gradient of vorticity magnitude with upwind bias was required in the original form.

A detailed rationale is given in Sec.1 of Ref.(13), included as Appendix I. Results for both convecting scalars and vortices in 2-D incompressible flow are given in Sec.2 of that paper.

For concentrated, convecting passive scalars, a new result is proven - a type of "Ehrenfest Theorem" which shows that the centroid of the scalar feature convects with the mean velocity, defined as an average velocity over the feature weighted by the amplitude of the scalar. Additional discussions are presented in Sections 1.5 and 1.6 of Ref.(14), included as Appendix II.

IV. Validation Studies - Original Vorticity Confinement

Three computations have recently been done to validate the original Vorticity Confinement method for realistic 3-D flows.

IV.1

The first involves flow over a rotorcraft landing ship. There, the vortex created at the leading edge corner of the deck in a even moderate cross-wind can convect over the deck, remaining strong and concentrated. This creates hazards for the landing rotorcraft. Results are presented in Ref.(15) and Ref.(16) (included as Appendix III).

In section 3.2 of the latter, it can be seen, first, that Vorticity Confinement was necessary even to get reasonable results, with the computational grid used. Second, it can be seen that the vortex position and induced velocity are very close to that measured experimentally.

IV.2

Two canonical 3-D turbulent blunt body flows were computed and compared with experiment. These involved flow over a circular cylinder at a Reynolds number of 3,900 and a square cylinder at a Reynolds number of 21,400. Results of the first were presented in Ref. (15) and Ref. (14) (included as Appendix III). The square cylinder results were also presented in the latter.

The main goal of this study was to investigate the promise of Vorticity Confinement as a way to effectively and economically model the small scale vortices in a turbulent wake flow. This was a very different case than previous trials which involved isolated, concentrated vortices and surface shear layers, since a large range of scales was involved. This study, then, evaluated Vorticity Confinement as a very simple, effective alternative Large Eddy Simulation (LES) method. Only a simple parameter, the confinement multiplier, "ϵ" was

used to model Reynolds number effect, which was held constant throughout the field. As ϵ was increased, the small scales and velocity fluctuations became more energetic.

In Sec. 3 of Ref. (16) (Appendix III), the changes in the rms fluctuating velocity profiles can be seen as ϵ is varied. For both circular and square cylinders, a value of ϵ was easily found such that both mean and rms velocity profiles matched experiment extremely closely. We are currently searching for measurements at other Reynolds numbers to calibrate ϵ. It surprised us that only the single confinement term, with one parameter seemed to serve as an effective LES model. We believe that our ability to capture small scale vorticies over only ~ 2 grid cells gave us a large enough range of scales, even on the moderate grid used, to accurately capture the larger scale turbulent dynamics. This is possible because we use an inherently discrete, nonlinear model directly on the grid. This is very different from conventional LES schemes which attempt to model the small scale structures with model partial differential equation (pde) terms. These pde's must then be resolved by finite different schemes, which require many more grid points.

V. Extended Surface Boundary Layer Treatment

V.I

The main part of the current project involved developing a computational method for blunt bodies in incompressible flow where the body could be simply represented by surface coordinates and "immersed" in a uniform, coarse Cartesian grid.

The first part involved the outer, inviscid flow. This was accomplished in a simple way using a level set description of the surface, and Vorticity Confinement to remove interpolation errors (which show up as numerical vorticity) in the region near the surface. The new feature here is that an inviscid "model" was used near the surface eliminating the first order numerical boundary layer created with the original method, resulting in a much more accurate solution.

The second part of the project involved viscous separation. This was readily treated in an approximate way by the original Vorticity Confinement method with no-slip boundary conditions at the surface. To increase the accuracy and allow additional terms to be added to create an effective turbulent boundary layer model that could be easily calibrated a "Surface Boundary Layer Model" (SBLM) was developed that was matched to the new inviscid near-surface "inviscid model" and did not depend on the orientation of the surface with respect to the main Cartesian grid. This allowed the modeling of the boundary layer separation in a grid-independent way. Preliminary results using a single surface velocity equation are reported in Sec. II.

Frank Caradonna (17) brought up the point that good results have been obtained for surface separation using Vorticity Confinement in this case for dynamic stall[18] - a difficult problem. This study used a body fitted grid where the boundary layer was confined by the Vorticity Confinement to ~ 2 cells near the surface - effectively forming an SBLM. Due to the body conforming grid there it was, of course, independent of surfce orientation. He suggested trying to use such an approach (only very near the surface), since it had been

shown to be effective.

For this reason, we recently have implemented this approach. Even though it uses a "body fitted grid", this is trivial to create since it is confined to the near surface region and only requires extending the surface defining coordinates by a small amount. The solution on this grid is then matched to our "outer" inviscid solver. We are finding that this method is much less sensitive than our original, "single surface variable" method, though it still is, effectively, a surface method, but with 2-3D velocity variables (grid planes). It allows independent verification/testing of the surface model, include post-separation. It also allows contact with body-fitted dynamic stall work.

Initial results (using a much finer near-body grid than necessary) for a circular cylinder are presented in Fig. 10 and 11 for the flow on the inner planes. Note that just the first 2-3 planes take part in initial separation - this is the "Extended" SBLM. The full outer grid flow resulting from the separation is shown in Fig. 12. The diameter of the circular cylinder was 16 unit grid cells. The outer grid has 128×128 unit grid cells and the inner grid has $20(radius) \times 50(circumferential)$ grid cells (with the cell size $dr = 0.1$ and $d\theta = 2\pi/50$). The time step for outer and inner region are 0.2 and 0.02 respectively. Results shown was after 100 time steps. μ for the outer and inner region are 0.75 and 0.05 respectively and ϵ for the outer and inner region are 1.125 and 0 respectively.

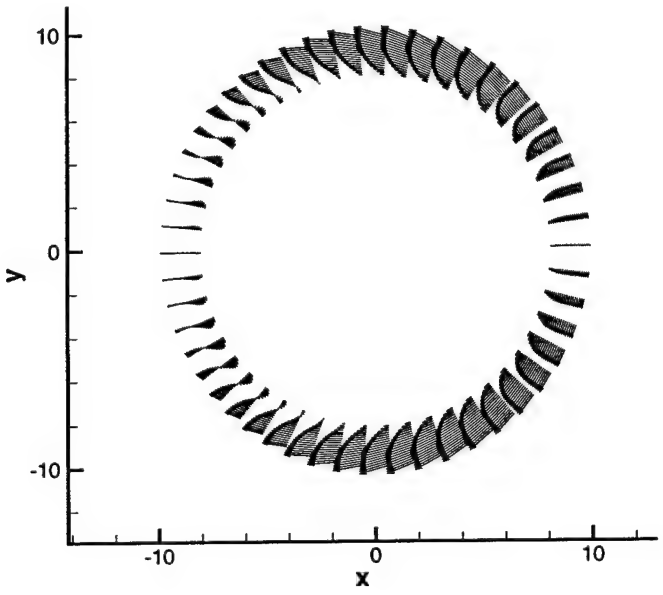

Figure 10: Velocity Vector of the Inner Region for Flow Over Circular Cylinder (without interaction with outer region)

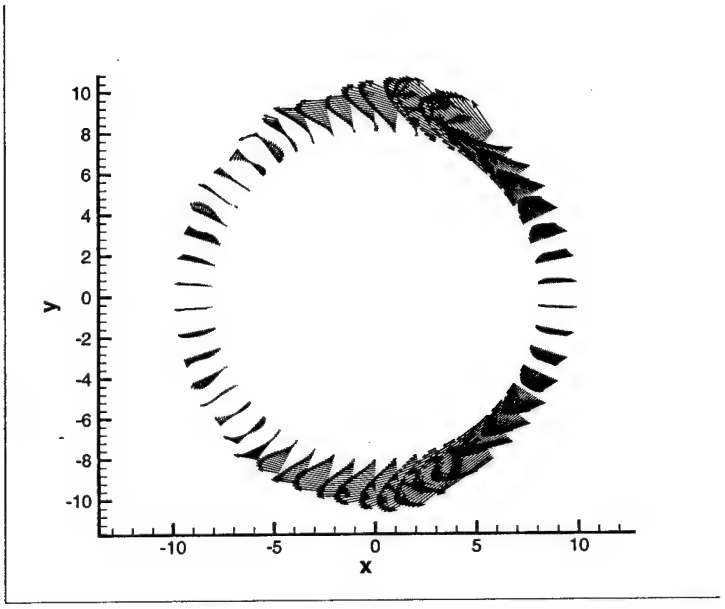

Figure 11: Velocity Vector of the Inner Region for Flow Over Circular Cylinder

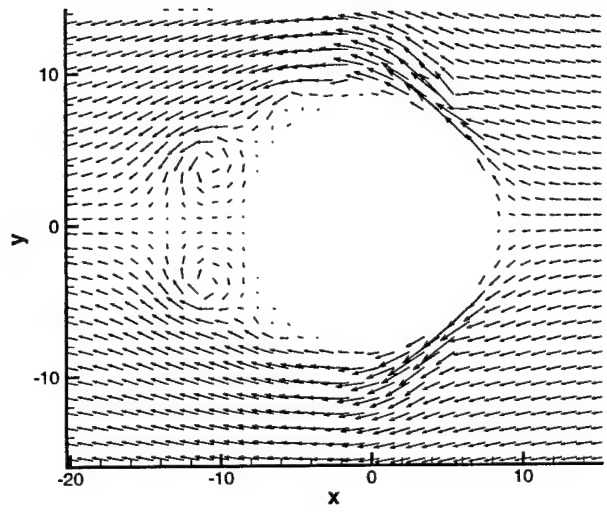

Figure 12: Velocity Vector for the Flow Over Circular Cylinder

V.2 Conclusion of Section

An extended SBLM approach was shown to be effective. Now, additional model terms can be added in a robust - grid independent way - while still immersing the surface in a simple, uniform Cartesian grid. Additional, more complex configurations, including a 3-D prolate ellipsoid are being studied.

VI. References

1. "Application of Vorticity Confinement to the Prediction of the Flow over Complex Bodies - A Survey of Recent Results", W. Dietz, M. Fan, J. Steinhoff, Y. Wenren, AIAA-2001-2642.

2. "Vorticity Confinement: An Efficient Eulerian Method for Computing High Reynolds Number Incompressible Flows", John Steinhoff, Yonghu Wenren, Meng Fan, *8th Annual Conference of the CFD Society of Canada*, June 11-13, 2000.

3. "Efficient Eulerian Computation of Realistic Rotorcraft Flows Using Vorticity Confinement - A Survey of Recent Results", Y. Wenren, M. Fan, W. Dietz, G. Hu, C. Braun, J. Steinhoff, B. Grossman, AIAA-2001-0996.

4. 2^{nd} ARO Workshop on Vorticity Confinement, UTSI, May. 1997.

5. 3^{rd} ARO Workshop on Vorticity Confinement, UTSI, Oct. 1998.

6. 4^{th} ARO Workshop on Vorticity Confinement, UTSI, Nov. 2, 2000.

7. "Self-Sustaining Mechanisms of Wall Turbulence", Editor: Ronald L. Panton, *Advances in Fluid Mechanics*, Vol.**15**, Computational Mechanics Publications 1997.

8. Private Communication, Dr. Alan Egolf.

9. "Linear And Nonlinear Waves", G.B. Whitham F.R.S., A Wiley-Interscience Publication, John Wiley & Sons, 1974.

10. "The Spontaneous Generation of the Singularity in a Separating Laminar Boundary Layer", L.L. Van Dommelen and S.F. Shen, Journal of Computational Physics, Vol.**38**, 1980.

11. "Theoretical Aerodynamics", Louis Melveille Milne-Thomson, Dover Publications, ISBN:048661980X, 1973.

12. "Application of Vorticity Confinement to the Prediction of the Flow over Complex Bodies," Wenren, Y., Steinhoff, J., Wang, L., Fan, M., and Xiao, M., AIAA Paper No. 2000-2621, Fluids 2000, Denver, CO, June, 2000.

13. "Convection of Concentrated Vortices and Passive Scalars as Solitary Waves", Steinhoff, J., Fan, M. and Wang, L., UTSI preprint, Submitted for SIAM Journal of Scientific Computing,2002.

14. "Vorticity Confinement- Recent Results: Turbulent Wake Simulations and A New, Conservative Formulation", Steinhoff, J., Fan, M., and Wang, L., to appear in Frontiers of Computational Fluid Dynamics 2002.

15. "Computing Complex Flows on Coarse Grids Using Vorticity Confinement", Fan, M., Dietz, W., Wenren, Y., and Steinhoff, J., AIAA-2002-0135.

16. "Computing Blunt Body Flows On Coarse Grids Using Vorticity Confinement", Fan, M., Wenren, Y., Dietz, W., Xiao, M., Steinhoff, J., to appear in Journal of Fluids Engineering, December, 2002.

17. Private Communication, Caradonna, F., Army Aeroflight Dynamics Group, Moffett Field, CA, 2002.

18. "A Technique for the Simulation of Stall with Coarse-Grid CFD", Moulton, M., and Steinhoff, J., AIAA-00-0277 (2000).

Appendix I

CONVECTION OF CONCENTRATED VORTICES AND PASSIVE SCALARS AS SOLITARY WAVES

John Steinhoff*, Meng Fan% and Lesong Wang$

University of Tennessee Space Institute, Tullahoma, TN

Submitted to the Journal of Scientific Computing, May, 2002

Abstract

A new computational method is described that efficiently treats thin features in multi-dimensional incompressible fluid flow, such as vortices and streams of passive scalars, and convects them over long distances with no spreading due to numerical errors. Outside the feature, where the flow is irrotational or the scalar vanishes, conventional discretized finite difference fluid dynamic equations are solved. The feature is treated as a type of weak solution and, within the feature, a nonlinear *difference* equation, as opposed to *finite difference* equation, is solved that does not necessarily represent a Taylor expansion discretization of a simple partial differential equation (pde). The approach is similar to shock capturing, where conservation laws are satisfied, so that integral quantities such as total amplitude and centroid motion are accurately computed for the feature. A more general approach is needed, however, than for conventional shock capturing, which are basically 1-D phenomena. Basically, we treat the features as multi-dimensional nonlinear discrete solitary waves that live on the computational lattice. These obey a "confinement " relation that is a rational generalization to multiple dimensions of 1-D discontinuity capturing schemes.

We have already been working for several years with a method – "Vorticity Confinement" that creates solitary waves on the lattice over only 2-3 grid cells and efficiently solves these problems, and have generated a large number of results for basic and complex, realistic flows. The main objective of this paper is to introduce a completely new formulation, that, compared to the original formulation, is simpler, allows more detailed analysis, and results in more compact structures for both vortices and convecting scalars.

First, some practical motivations are described. Then, a short critique of conventional methods for these problems is given. The basic new method is then described. Some analysis of the new method and initial results are finally presented.

---

* Professor

% Research Scientist

$ Graduate Research Assistant

1. Introduction

A new computational method is described that efficiently treats thin features in multi-dimensional incompressible fluid flow, such as vortices and streams of passive scalars, and convects them over long distances with no spreading due to numerical errors. Outside the feature, where the flow is irrotational or the scalar vanishes, conventional discretized finite difference fluid dynamic equations are solved. The feature is treated as a type of weak solution and, within the feature, a nonlinear *difference* equation, as opposed to *finite difference* equation, is solved that does not necessarily represent a Taylor expansion discretization of a simple partial differential equation (pde). The approach is similar to shock capturing [1], where conservation laws are satisfied, so that integral quantities such as total amplitude and centroid motion are accurately computed for the feature. A more general approach is needed, however, than for conventional shock capturing, which are basically 1-D phenomena. Basically, we treat the features as multi-dimensional nonlinear discrete solitary waves that live on the computational lattice. These obey a "confinement " relation that is a rational generalization to multiple dimensions of 1-D discontinuity capturing schemes (this is elaborated on in the Appendix).

Differences, compared to conventional shock capturing, are that:

First, unlike shocks, characteristics do not point into the feature, and extra terms must be designed to prevent it from spreading due to numerical effects in the convection. (Harten [2] developed such a scheme, but for contact discontinuities in 1-D compressible flow.)

Second, shocks are basically one dimensional discontinuities, unlike vortex filaments or thin streams of passive scalars, which are intrinsically multi-dimensional: A concatenation of 1-D "capturing" operators along separate axes will not, generally, give smooth solutions. Due to the multidimensional nature, it seems necessary to pay attention to the structure within the feature, even though it is sampled on only a few grid cells in the cross-section.

We have already been working for several years with a method – "Vorticity Confinement" that efficiently creates solitary waves on the lattice and efficiently solves these problems, and have generated a large number of results for basic and complex, realistic flows [3-12]. The main objective of this paper is to introduce a completely new formulation, that, compared to the original formulation, is simpler, allows more detailed analysis, and results in more compact structures for both vortices and convecting scalars.

First, some practical motivations are described. Then, a short critique of conventional methods for these problems is given. The basic new method is then described. Some analysis of the new method and initial results are finally presented.

1.1 Motivation

There are many important fluid dynamic problems where thin, concentrated flow features must be numerically convected over long distances. Examples include vortices shed from forebodies and lifting surfaces of aircraft , rotorcraft and submarines, and thin streams of contaminants convecting in ambient flow. Often, for these cases, the main

interest is the integrated amplitude through the feature and the motion of the centroid, rather than the details of the internal structure. In general, these features can originate in many places, reattach, merge, and have complex topology. Accordingly, we consider Eulerian methods where very general topologies can be treated, as opposed to Lagrangian "particle tracking" methods.

1.2 Current Methods

Conventional Eulerian approaches to the convection problem for incompressible flow involve formulating governing pde's, discretizing them and solving them as accurately as possible on feasible computational grids, assuming only strong solutions. For smooth, non-thin features, these methods are well known to converge to the correct solution as the number of points across the feature in a typical direction, N, becomes large: Error estimates are asymptotic in N. For accurate solutions, even higher order, complex discretization methods typically require N to be at least ~8 or 10 so that the error obeys the large N estimate. Even then, it is well known that solutions degrade over long convection distances (many time steps). As a result, although conventional methods may be efficient, for example, for low Reynolds number flow problems with large smooth vortical regions, they are inefficient (or not even feasible) for thin aircraft trailing vortices convecting over long distances.

It appears that adaptive, unstructured grids cannot improve the resolution significantly for realistic problems with many thin features. Also, even for small numbers of time dependent features these methods are very expensive, compared to uniform grid, structured methods.

For these reasons, for the problems considered, it is important to have only very few (2 or 3) grid points across each feature if it is very thin, and to convect it with no numerical spreading. This small number of grid points is consistent with the stated desire to only compute a few integral quantities across the feature, such as total amplitude and centroid position. Then, the difference scheme can, effectively, serve as a simple, implicit "solitary wave" model for the internal structure. However, as explained above, this is not feasible with conventional pde-based methods. As an example of the limitations of conventional methods, if we are limited to, say, a $(128)^3$ computation and use a conventional method which requires ~8 cells to avoid excessive numerical spreading, it may then be reasonable to say that the smallest "computational scale", Δ, is 8/128 or 1/16, rather than the desired scale of ~ 2/128 or 1/64. Scales much smaller than 1/16 will be strongly damped and features will quickly spread due to numerical effects if a pde is to be resolved. This difficulty shows up as a limit on the effective number of degrees of freedom of the simulation, which is reduced by a factor of $\sim 4^3$, if a conventional method is compared to one with an actual 2 cell small scale resolution.

2. Vorticity Confinement Approach

As stated, over the last several years a new method was developed to treat problems with thin, convecting vortices [3-12]. This method, termed "Vorticity

Confinement", is intrinsically multidimensional and, although equally applicable to thin vortices and (in modified form), thin streams of passive scalars, almost all of its uses have involved vorticity. First (through Sec. 2.1), a section of ref. [3] (with some changes) will be included that describes the basic features of Vorticity Confinement. Then, the new formulation will be introduced, and new analyses and results involving the application of the method to convecting vortices and scalars presented.

Vorticity Confinement is a method to preserve convecting, concentrated vorticity on a coarse grid; the vortical structures can represent boundary layers over solid surfaces, the smaller scales (of the order of a grid cell) in turbulent wakes, or separated, thin vortex filaments that convect over arbitrarily long distances. Vorticity Confinement can be implemented in a pre-existing flow solver, for both incompressible and compressible flow, by adding a term to the discretized momentum conservation equations [4]. The same basic approach, applied to convecting scalars, will also be described below.

For general unsteady incompressible flows, the governing equations with the Vorticity Confinement term are discretizations of the continuity equation and the momentum equations, with an added term:

$$\nabla \cdot \vec{q} = 0$$

$$\partial_t \vec{q} = -(\vec{q} \cdot \nabla)\vec{q} - \frac{1}{\rho}\nabla p + h^2[\mu \nabla^2 \vec{q} + \varepsilon \vec{s}]/\Delta t \qquad 2.0$$

where $\vec{q}$ is the velocity vector, p is the pressure, ρ is the density, and μ is a diffusion coefficient that includes numerical effects (we assume physical diffusion is much smaller), and the discretized grid cell size is h and time step, Δt. For the last term, $\varepsilon\vec{s}$, ε is a numerical coefficient that, together with μ, controls the size and time scales of the convecting vortical regions or vortical boundary layers. For this reason, we refer to the two terms in the brackets as "confinement terms".

The basic idea is that we want the computed thin features to maintain shape and total amplitude as their centroid is convected through the flow field. The requirement that they relax to their shape in a small number of time steps and have a support of a small number of grid cells determines the two parameters, ε and μ. Also, the "outer" flow field in which the feature is convecting is slowly varying in time and space compared to these scales (this is required if the grid cell size and time step are to resolve the pde's governing this outer flow). We then have a two-scale problem with the thin vortex or scalar obeying a "fast" dynamics.

$$\mu \nabla^2 \vec{q} + \varepsilon \vec{s} \approx 0,$$

where $\vec{s}$ is defined below in Sec. 2.1.

Thin vortices are then convected through the flow field by the "slow" variables, $\vec{q}$ (with the self-induced velocity, which does not affect the motion of the centroid of the vortex, subtracted). Exactly the same type of discussion applies to the convection of a passive scalars, as described below.

In general, for convecting vortex filaments, computed flow fields *external* to the vortical regions are not sensitive to the parameters ε and μ over a wide range of values.

For example, the flow outside an axisymmetric 2-D vortex core is independent of the vortical distribution, and hence does not depend on ε and μ as long as the core is thin. Hence, the issues involved in setting them are similar to those involved in setting numerical parameters in other standard computational fluid dynamics schemes, such as artificial dissipation in many conventional compressible solvers. There, the flow outside 1-D captured shock regions does not depend on the exact internal structure, as long as it is thin.

An important feature of the Vorticity Confinement method is that the Confinement terms are non-zero only in the vortical regions, since both the diffusion term and the anti-diffusion term vanish outside those regions (care has to be taken in the numerical implementation to preserve this feature).

Another important feature concerns the total change induced by the confinement correction in mass, vorticity and momentum, integrated over a cross section of a convecting vortex. It can be shown [7-9] that mass is conserved because of the pressure projection step in the solver and vorticity is explicitly conserved because of the vanishing of the confinement term outside the vortical regions. For the original confinement formulation used previously, momentum was almost exactly conserved. A previous extension of the original method [5,10], explicitly conserved the momentum, but resulted in a more spread vortex and implementation was somewhat complex. The new formulation, described below, explicitly conserves momentum, is much simpler, and results in more compact structures.

2.1 New Vorticity Confinement Formulation

First, the new formulation for scalar confinement will be given. Then, a velocity-based (primitive variable) Vorticity Confinement term given that exactly reduces to the new scalar confinement (in terms of vorticity) when the curl is taken. The scalar formulation presented here is related to that presented in [11] in 1-D. In this section no convection is used, only the two confinement terms, so that the behavior can be seen more clearly. Excellent results are found with convection and will be shown in Sec. 3 for vorticity as well as convecting scalars.

We start with an iteration for a non-negative scalar, ϕ :

$$\phi^{n+1} = \phi^n + \mu h^2 \nabla^2 \phi^n - \varepsilon h^2 \nabla^2 \Phi^n \qquad 2.1.1$$

where

$$\Phi^n = \left[\frac{\sum_l C_l (\tilde{\phi}^n)^{-1}}{\sum_l C_l} \right]^{-1} \qquad 2.1.2$$

$$\tilde{\phi}^n = |\phi|^n + \delta$$

where the sum is over a set of grid nodes near and including the node where Φ is computed, the absolute value is taken and δ, a small positive constant ($\sim 10^{-8}$) is added to prevent problems due to finite precision. The coefficients, C_l, can depend on l, but good results are obtained by simply setting them all to 1 (except for a convecting scalar, as explained in Sec. 3.2. Eq. 2.1.2 is related to the harmonic mean [13].

For example, in 2-D, except for convecting scalars, the form used in this study is

$$\Phi_{ij}^n = \left[\frac{\sum_{\alpha=-1}^{+1} \sum_{\beta=-1}^{+1} \left(\tilde{\phi}_{i+\alpha, j+\beta}^n \right)^{-1}}{N} \right]^{-1}$$

where the number of terms in the sum is N=9. Different values were used for convecting scalars, as explained in Sec. 3.2.

Here, we assume $\phi^n \geq 0$. Negative values can also be accommodated with a small extension. Both μ and ε are positive.

An important feature is that all terms are homogeneous of degree 1 in Eq. 2.1.1. This is important because the confinement should not depend on the scale of the quantity being confined. Another important feature is the nonlinearity. It is easy to show that a linear combination of terms, for example of second and fourth order, cannot lead to a stable confinement for any finite range of coefficients.

For smooth ϕ fields (long wavelengths), the last term represents a diffusion of order $n^2 / \Delta t$, i.e., it is first order accurate if Δt is proportional to h. If $\mu \leq \varepsilon$, the total diffusion (in the long wavelength limit) is negative. However, the iteration of Eq. 2.1.1 is still stable and converges for values of ε up to about 5μ. Also, the discrete, converged solution as $n \to \infty$ can be given exactly in terms of sech functions (to be described in the next section).

The next step in our development involves letting ϕ be the magnitude of vorticity and deriving an equation for the corresponding primitive variable velocity term that leads to Eq. 2.1.1 when the curl is taken (exactly in 2-D, or for a straight vortex in 3-D). This will result in a new formulation of Vorticity Confinement. In 3-D, if the curvature of a vortex filament is large compared to its thickness, the results will still be approximately valid since then the flow is close to that of a 2-D vortex in a plane normal to the filament.

We define

$$\vec{q}^{\,n+1} = \vec{q}^{\,n} + \mu h^2 \nabla^2 \vec{q}^{\,n} + \varepsilon h^2 \vec{s}^{\,n}$$
$$\vec{s} = \vec{\nabla} \times \vec{w} \qquad 2.1.3$$

Since $\vec{\nabla} \cdot q = 0$, we can write

$$\vec{q}^{\,n+1} = \vec{q}^{\,n} - h^2 \vec{\nabla} \times \left(\mu \vec{\omega}^{\,n} - \varepsilon \vec{w}^{\,n} \right)$$

where

$$\vec{\omega}^n = \vec{\nabla} \times \vec{q}^n$$

and

$$\vec{w}^n = \frac{\vec{\omega}^n}{\tilde{\omega}^n}\left[\frac{\sum_l (\tilde{\omega}_l^n)^{-1}}{N}\right]^{-1} \qquad 2.1.4$$

where $\tilde{\omega}_l^n = \left|\vec{\omega}_l^n\right| + \delta$

and the sum is the same as in Eq. 2.1.2.

We are currently implementing the new method in our general fluid dynamic codes. In addition, the use of the "Scalar Confinement" version, Eq. 2.1.1, is being used for flows where thin streams of passive scalars, such as contaminants, must be convected over long distances.

2.2 Analysis of Zero Convection Form

When convection and (for vorticity) pressure terms are included, the results of Sec. 2.1 may change. For example, if one convection step is followed by one confinement step, the results may be different, even in a frame convecting with the feature. However, according to our earlier 1-D studies [11], we still expect a steady state distribution to be reached in the convecting frame. Further, if desired, we should be able to relax to the above zero convection form each time step by performing a number of confinement operations after each convection operation or simply take Δt small (continuous time, discrete space limit). Thus, it is important to analyze this form.

Taking the scalar case, assuming convergence as $n \to \infty$, we have

$$\nabla^2(\mu\phi - \varepsilon\Phi) = 0,$$

If ϕ (and hence Φ) vanishes outside the feature, we have $\mu\phi_0 = \varepsilon\Phi$,
where the point (i, j) is given the label $l = 0$, or

$$\phi_0^{-1} - \frac{\mu}{\varepsilon N}\sum_l \phi_l^{-1} = 0$$

we take

$$\phi_{ij} = \frac{1}{4} A \sec h[\alpha(x_i - x_0)] \sec h[\alpha(y_j - y_0)], \qquad A,\ x_0,\ y_0 \text{ constant},$$

and where $x_i = ih$, $y_j = jh$, h is the grid cell size, and use the form corresponding to $C_l = 1$ in Eq. 2.1.2. We then have

$$\phi_{ij}^{-1} = AX_iY_j, \qquad X_i = e^{\alpha hi - \alpha x_0} + e^{-\alpha hi + \alpha x_0}, \quad Y_j = e^{\alpha hj - \alpha y_0} + e^{-\alpha hj + \alpha y_0}$$

Then, for any values of A, x_0 and y_0,

$$(X_{i+1} + X_i + X_{i-1})(Y_{j+1} + Y_j + Y_{j-1}) - \frac{\varepsilon N}{\mu} X_i Y_j = 0$$

or

$$(e^{\alpha h} + 1 + e^{-\alpha h})(e^{\alpha h} + 1 + e^{-\alpha h}) - \frac{\varepsilon N}{\mu} = 0$$

Hence,

$$ch(\alpha h) = \frac{1}{2}[(\frac{\varepsilon N}{\mu})^{\frac{1}{2}} - 1],$$

which determines α. This implies that there is only a solution for $\varepsilon > \mu$, since $N = 9$ here. Of course, stability has not been proven here.

2.3 Solution with Convection

It is important to realize that the confinement steps do not alter the total momentum, vorticity or total amount of a scalar (assuming vorticity or scalar concentration has finite support). Also, the centroid is not changed. This is easy to show, not only in the continuum limit but also for the discrete equations, since the confinement terms are second derivatives. The following argument assumes, for each convection step (n), there is at least one confinement step so that the feature remains compact. If ϕ represents a confined passive scalar or vorticity magnitude, then, using our conservative convection routine, we have the following relationships for the dynamics of the convecting solitary wave (we describe the 2-D case for simplicity):

For the convecting passive scalar, we have a discretization of

$$\partial_t \phi = -\bar{\nabla} \cdot (\vec{q}\phi) + h^2 \nabla^2 (\mu\phi - \varepsilon\Phi)/\Delta t$$

assuming $\bar{\nabla} \cdot \vec{q} = 0$. Then,

$$\phi^{n+1} = \phi^n - \Delta t \bar{\nabla}_{disc.} \cdot (\vec{q}\phi) + h^2 \nabla^2_{disc.} (\mu\phi - \varepsilon\Phi)$$

where discrete operators are labeled.
For conservative discretization, the total amplitude

$$< \Phi > \equiv \sum_{ij} \phi_{ij}^n$$

is independent of n. If we define the centroid

$$< \vec{X} >^n \equiv \sum_{ij} \vec{x}_{ij}^n \phi_{ij}^n / < \Phi >$$

and the weighted mean velocity

$$< \vec{q} >^n \equiv \sum_{ij} \vec{q}_{ij}^n \phi_{ij}^n / < \Phi >$$

where $\vec{x}_{ij}$ is the (fixed) position vector of node (i, j), and ϕ_{ij} and $\vec{q}_{ij}$ are the scalar value and the velocity at that node, then the centroid evolves according to:

$$< \vec{X} >^{n+1} = < \vec{X} >^n + \Delta t < \vec{q} >^n$$

For vortices, the self-induced velocity which is included in the above sum exactly cancels and, as in the passive scalar case, the $\vec{q}_{ij}$ can be taken to be an externally applied (irrotational) velocity. The above result then still holds.

Since we are, at this point, only interested in the "expectation values" of scalars or vorticities for thin features and that the features remain compact, spread over only a few cells, this Ehrenfest-type relation is exactly what we need. Only the variables of importance are, effectively, solved for. This shows that the features, when isolated, evolve as particles with essentially no internal dynamics. However, we keep the very important Eulerian feature that the number of features is not fixed. We could, for example, create additional solitary waves by inserting a source: No additional computational markers need be created, as in Lagrangian schemes. For this study, we show that features can automatically merge and reduce in number. This will be seen in the results of Sec. 3. As for the earlier Vorticity Confinement method, this property is crucial for the general treatment of interacting vortical regions, especially in 3-D [5,9,10,12].

3. Results

All results presented are in 2-D. Also, all convection cases use a conservative second-order centered convection term together with a centered diffusion term and are first-order-explicit in time. In all the result plots, axes are labeled with grid node location. Plots of amplitude are made using dense contours with white grid lines superimposed.

3.1 Zero Convection

Results are presented in Fig. 1 after 0, 8, and 100 iterations, for vorticity and velocity for a vortex in 2-D. Values used were $\mu = .2$, $\varepsilon = 0$ and $\varepsilon = 5\mu$. In this figure, the vorticity contour levels extend from about ¼ of the maximum initial value to the

maximum so that a measure of the size of the confined region can be determined. It can be seen that the confinement is very effective and stable.

3.2 Passive Scalar Convection

A good test involves convection of a small passive scalar pulse in solid-body rotating flow [14]. For this case a convection step was followed by a single confinement step (including diffusion). The full summation of Eq. 2.1.2 with $C_l = 1$ leads to a thin spreading of the pulses in the direction normal to their motion (This spreading does not occur for vortices, for reasons described in Sec. 3.3). This scalar spreading seemed to be due to the inclusion of "downwind" values, which is known to cause instability. We then simply set $C_l = 0$ for downwind points. The problem was almost completely cured, and only a very weak spreading remained, which could easily be cured, if desired.

Results are shown in Fig. 2a for a single pulse convecting through the 1st rotation (2π) and in Fig. 2b through 10th rotation. Contours are plotted from initial maximum value to 1/3 of that value. There are 157 time steps between pulse images ($\pi/8$ radius) and the final image was after 12,560 time steps. This represented a travel of 1,256 cells or about 433 pulse diameters. The open circle labels the starting location. The time step was not set to exactly divide the circuit so we would not expect the final image to exactly coincide with the initial one. However, the final position is within plottable accuracy of the calculated angle and radius. The final radius can be seen to be very close to the initial one. This is somewhat surprising since the method was only first order in time and second order in space. We have not yet attempted to reduce the small, residual cross-flow spreading. This could easily be accomplished with a small amount of additional negative diffusion in the cross-stream direction. For the case computed, we used $\mu = 0.15$, $\varepsilon = 0.75$.

Finally, a run was made with no confinement and a lower, (minimal) diffusion set for stability. The maximum amplitude decreased to below the plotting threshold after only $\pi/8$ radians of travel (position of the first image in Fig. 2a).

3.3 Vorticity Confinement

The incompressible fluid dynamic equations with Vorticity Confinement, Eq. 2.0, were discretized and solved. Each time step, the same convection scheme used for the above scalar was used. A standard pressure projection method was used to enforce incompressibility [15]. This used a staggered grid for pressure and velocity and a box scheme for the pressure gradient. The required Poisson equation for pressure was solved using a direct method "FishPack". Vorticity Confinement terms – Eqs. 2.1.3 and 2.1.4, were used, with $\mu = 0.05$, $\varepsilon = 1.5\mu$. Results were very close to these for $\mu = 0.2$, $\varepsilon = 1.5\mu$, implying that the method is not very sensitive to the values of these parameters. (Further investigaton of this point should be done). The time step, based on grid cell size and circumferential velocity near the vortex cores, was 0.4 and the grid had 128×128 cells. For vortices, the full summation (Eq. 2.1.2) with all $C_l = 1$ was used,

without excluding downwind points. This exclusion, useful for scalar convection, was not important here because the large circulating velocities near the vortex cores rapidly convected any cross-stream spread vorticity around the cores, keeping them close to axisymmetric. The confinement then kept the cores compact.

3.3.1

First, vortices of opposite sign were computed with no external free-stream-velocity, convecting only under their own induced velocities. Each time step the total amplitudes and centroids of both positive and negative vorticity were computed. The velocities induced by corresponding point vortices at these locations were computed on the boundaries as velocity boundary conditions, and Dirichlet conditions were used for pressure.

Results are presented in Fig. 3 for a sequence of time steps. The computed vortex centroids are convecting at the same velocity, to plottable accuracy, as if they were point vortices. The self-induced velocity in each vortex, although several times the convecting velocity of the centroid, automatically cancels and has no effect because the method conserves momentum, as explained in Sec. 2.3. The final images shown result from 1,800 time steps, yet the vortices are just as compact as initially. It should be mentioned that if the vortices are significantly closer, there will be an interaction and eventually vorticity will be exchanged. This is to be expected since there are "tails" of vorticity that (rapidly) decrease with radius beyond the region shown.

3.3.2

Vortices with the same sign were computed as they rotated around each other under their induced velocities. The vortices were initially (and finally) separated by 14 cells. First, the computation was done with no Vorticity Confinement, and with minimum diffusion required for convective stability. Contours are displayed in Fig. 4 corresponding to vorticity values between initial maximum and ¼ of that value. It can be seen that the vorticity rapidly diffuses. The computation was repeated with Vorticity Confinement. Values of μ and ε were those used in Sec. 3.3.1. Vorticity contours between initial maximum and ¼ maximum are displayed for 3 different times in the 1st loop around each other in Fig. 4a, and in the 20th loop in Fig. 4b. The behavior is as expected: The vortices can be seen to be essentially the same at the end (after 7,200 time steps) as initially.

The large variation in velocity in the space between the vortices can be seen in Fig. 5, both after 1 and after 20 loops. This would make it difficult for a pde-based Taylor expansion to give accurate results over long convection times.

As stated, the main reason for using an Eulerian method as opposed to Lagrangian is to allow vortices to merge and otherwise change topology, so that complex, realistic vortical configurations can be treated. This has been amply demonstrated by the original Vorticity Confinement method both in 2-D and 3-D [5,7,9,10,12]. To demonstrate that the new confinement method does not inhibit this merging we repeat the above computation, but with the vortices initially 5 cells apart. This is a repeat of a calculation

using the original Vorticity Confinement method [7]. It is known from vorticity contour or "waterbag" methods that corotating vortices become unstable and merge when they are initially closer than a few diameters. It can be seen in the vorticity contour plots of Fig. 6 that this merging automatically occurs, as expected, with the new Vorticity Confinement method.

Conclusion

A new Eulerian Vorticity Confinement has been introduced. Its advantages over the original Vorticity Confinement method are that it is simpler and easier to analyse and explicitly conserves total momentum. The method accurately convects thin features, either vortices or scalars, over very long distances, even though they are confined to only 2-3 grid cells. As in shock and other discontinuity capturing schemes, the details of the internal structure of the feature are not solved for, but implicitly modeled (the features are treated as weak solutions). Integral quantities, such as total amplitude and centroid, however, are accurately solved for. As such, the method essentially represents the features as nonlinear discrete solitary waves that live on the computational lattice. It is argued that the new method is a rational generalization of 1-D discontinuity confinement schemes to multiple dimensions.

Examples are presented for thin, convecting passive scalars and vortices in 2-D incompressible flow.

Acknowledgements

The first author acknowledges many helpful discussion with Barry Merriman and Stanley Osher. The work was supported by the Army Research Office and the University of Tennessee Space Institute.

References

[1] Lax, P.D., "Hyperbolic Systems of Conservation Laws II", Comm. Pure Appl. Math **10** (1957).

[2] Harten, A., "The Artificial Compression Method for Computation of Shocks and Contact Discontinuities III, Self-Adjusting Hybrid Schemes," *Mathematics of Computation*, Vol. 32, No. 142. April 1978.

[3] Fan, M., Wenren, Y., Dietz, W., Xiao, M., Steinhoff, J., "Computing Blunt Body Flows On Coarse Grids Using Vorticity Confinement", to appear in *Journal of Fluids Engineering*, December, 2002.

[4] Wenren,Y., Fan, M., Dietz, W., Hu, G., Braun, C., Steinhoff, J., and Grossman, B., " Efficient Eulerian Computation of Realistic Rotorcraft Flows Using Vorticity Confinement", AIAA-01-0996 (2001).

[5] Steinhoff, J., Wenren, Y., Braun, C., Wang, L., and Fan, M. "Application of Vorticity Confinement to the Prediction of the Flow over Complex Bodies", pp. 197-226 in *Frontiers of Computational Fluid Dynamics 2002* (D.A. Caughey and M.M. Hafez eds.); World Scientific, (2002)

[6] Fan, M., Dietz, W., Wenren, Y., and Steinhoff, J., "Computing Complex Flows on Coarse Grids Using Vorticity Confinement", AIAA-2002-0135.

[7] Steinhoff, J., Mersch, T., and Wenren, Y., "Computational Vorticity Confinement: Two Dimensional Incompressible Flow", Proceedings of the Sixteenth Southeastern Conference on Theoretical and Applied Mechanics. 1992.

[8] Steinhoff, J., Wang, Clin, Underhill, D., Mersch, T., and Wenren, Y., "Computational Vorticity Confinement: A Non-Diffusive Eulerian Method for Vortex-Dominated Flows," UTSI preprint, 1992.

[9] Steinhoff, J., "Vorticity Confinement: A New Technique for Computing Vortex Dominated Flows," In D.A. Caughey and M.M. Hafez, editors, *Frontiers of Computational Fluid Dynamics*. John Wiley & Sons, 1994.

[10] Wenren, Y., Steinhoff, J., Wang, L., Fan, M., and Xiao, M., "Application of Vorticity Confinement to the Prediction of the Flow over Complex Bodies," AIAA Paper No. 2000-2621, Fluids 2000, Denver, CO, June, 2000.

[11] Steinhoff, J., Puskas, E., Babu, S., Wenren, Y., and Underhill, D., "Computation of Thin Features Over Long Distances Using Solitary Waves," AIAA Proceedings, 13th Computational Fluid Dynamics Conference, July, 1997.

[12] Steinhoff, J. and Underhill, D., "Modification of the Euler Equations for Vorticity Confinement Application to the Computation of Interacting Vortex Rings," *Physics of Fluids*, 6, 1994.

[13] Stanley Osher, Private Communication.

[14] Orszag, S.A., "Numerical Simulation of Incompressible Flows Within simple Boundaries: Accuracy", *J. Fluid Mech.*, **49**, 1971.

[15] Kim, J., and Moin, P., "Application of a Fractional Step Method to Incompressible Navier-Stokes Equations", *Journal of Computational Physics*, Vol. **59**, 1995.

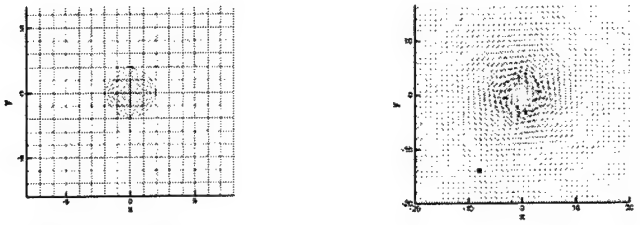

a) original condition

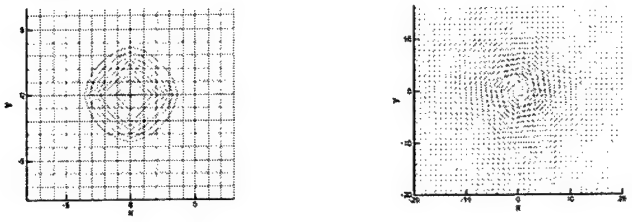

b) time steps = 8 $\varepsilon = 0$

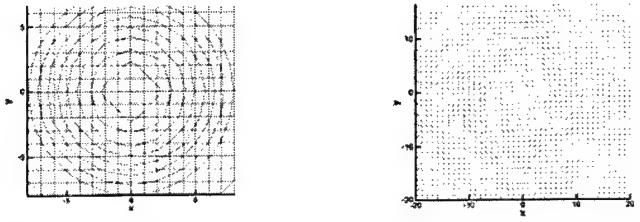

c) time steps = 100 $\varepsilon = 0$

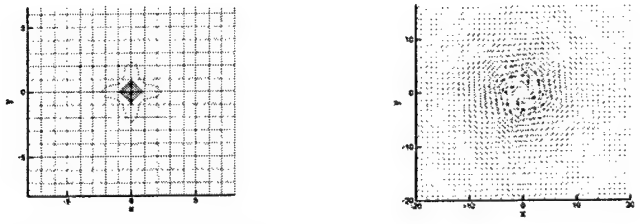

d) time steps = 8 $\varepsilon = 5\mu$

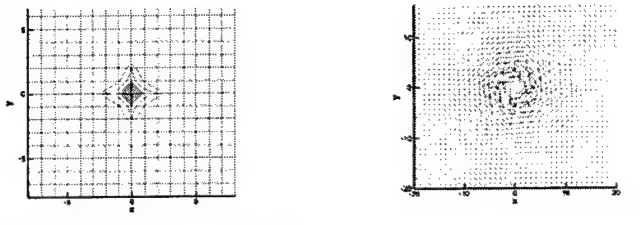

e) time steps = 100 $\varepsilon = 5\mu$

Figure 1 Vorticity contours and vector fields of velocity

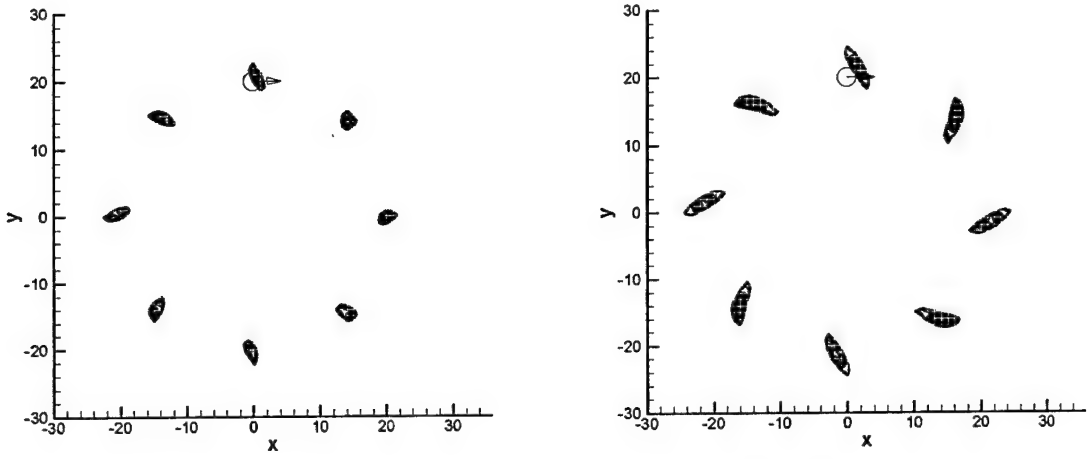

(a) 1st loop (b) 10th loop

Figure 2 Scalar convection

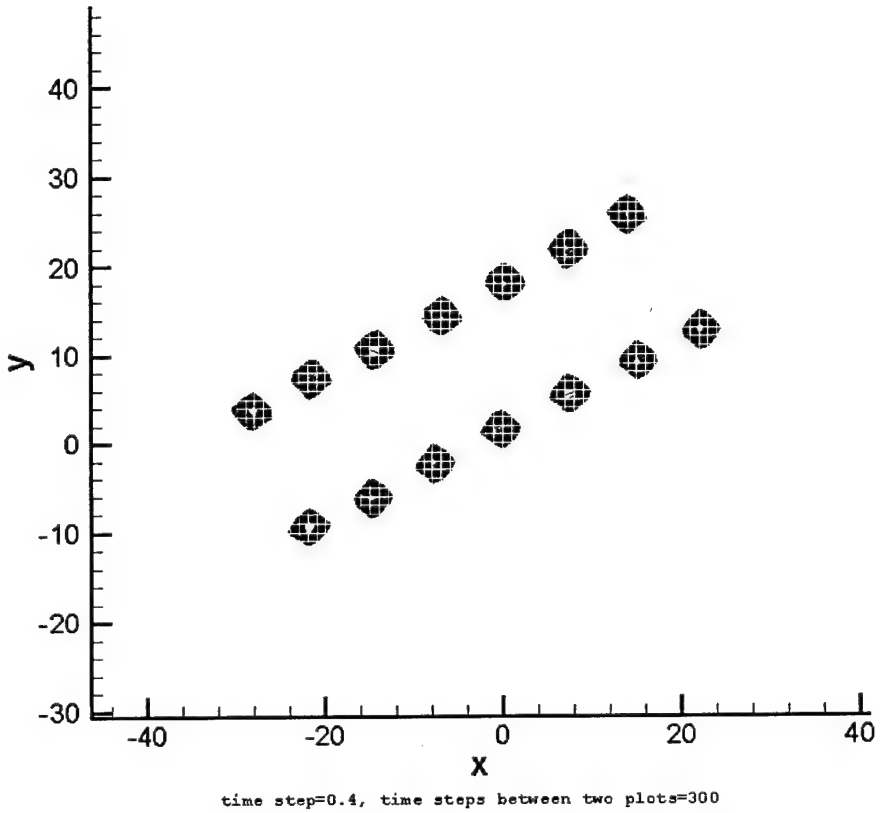

Figure 3 Vorticity contour plots of self-induced flow by two point vortices(15 cells apart) with opposite sign

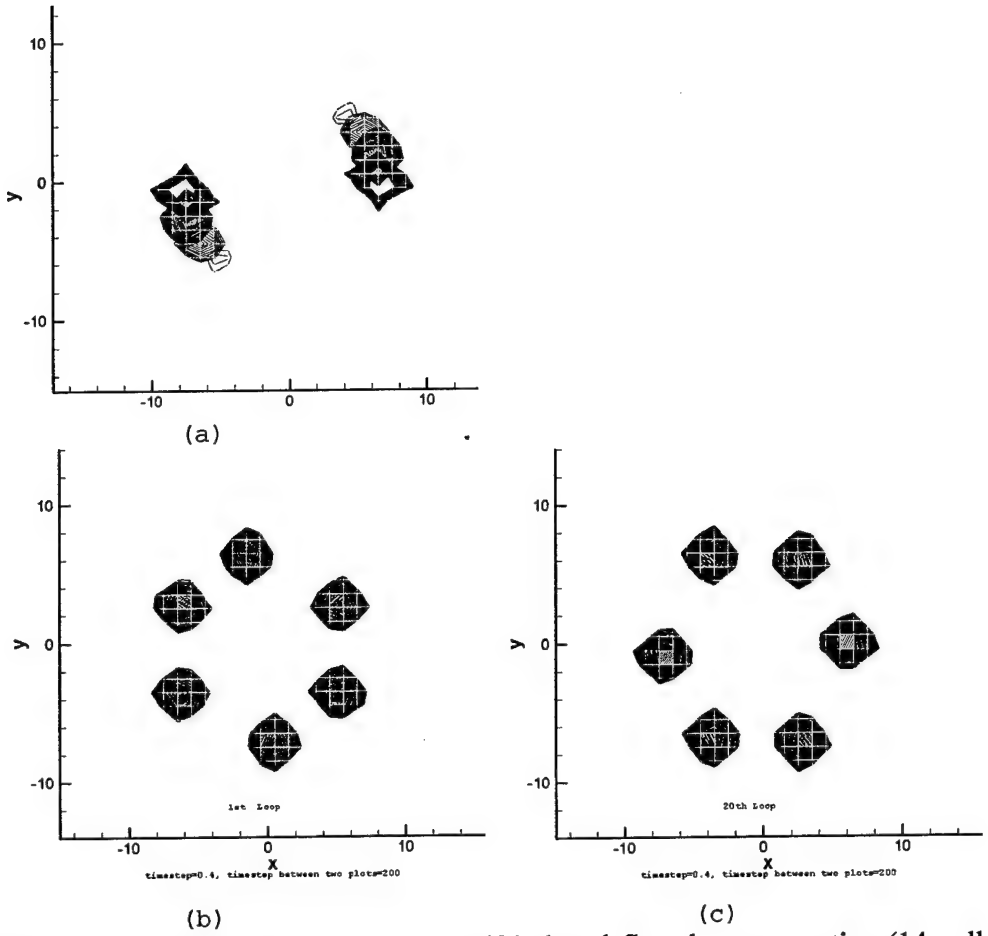

Figure 4 Vorticity contour plots of self-induced flow by two vortices(14 cells apart) with same sign. (a) without Vorticity Confinement; (b)with Vorticity Confinement, 1st loop; (c)with Vorticity Confinement, after 20th loops.

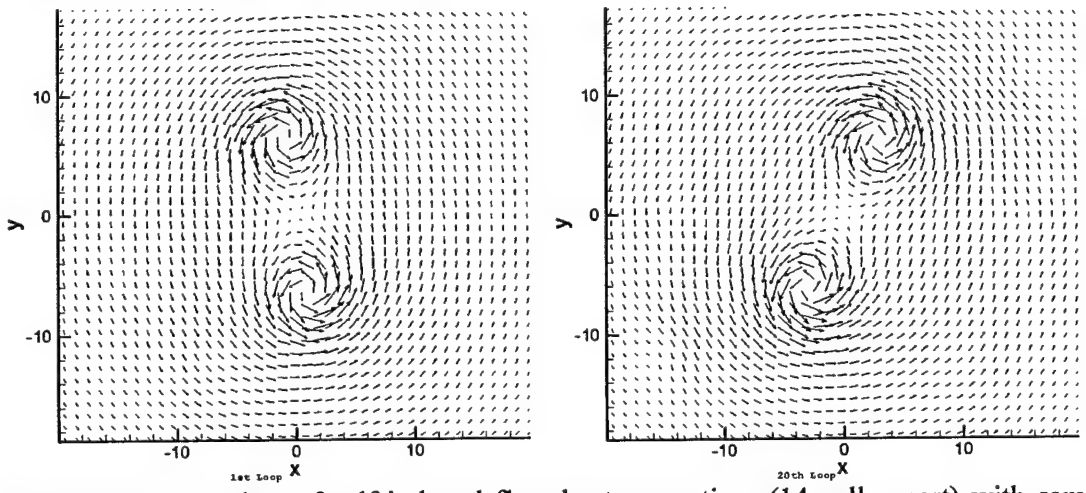

Figure 5 Vector plots of self-induced flow by two vortices (14 cells apart) with same sign. (a) with Vorticity Confinement, after 1 loop; (b) with Vorticity Confinement, after 20 loops.

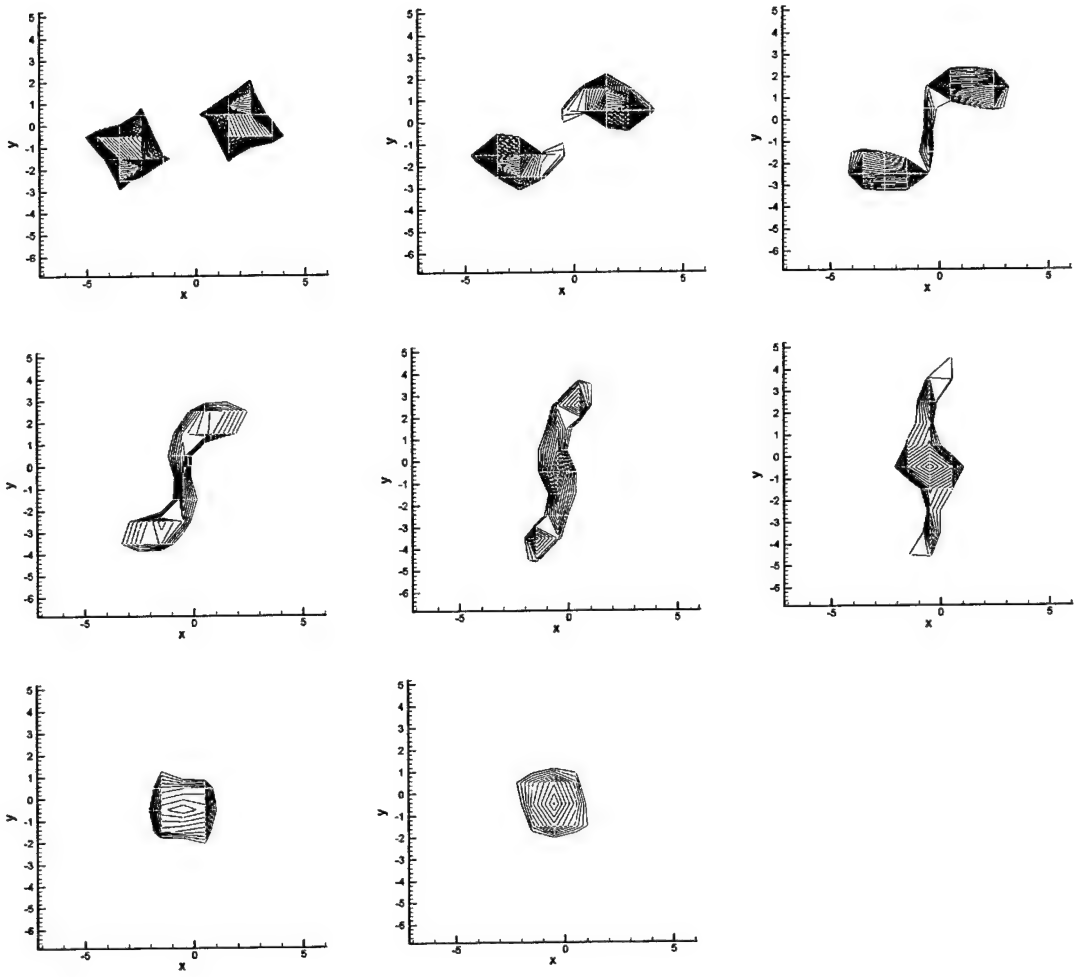

Figure 6 Vorticity contour plots of self-induced flow by two vortices(5 cells apart) with same sign, with Vorticity Confinement

Appendix

The new Vorticity Confinement method can be shown to be related to, and a generalization of, some recent 1-D discontinuity preserving schemes: In this Appendix we show that (a) For incompressible flow, the proper generalization to multidimensions of the first order derivatives used in 1-D discontinuity preserving schemes is the vorticity, which is the only non-zero rotationally invariant first order velocity derivative in 2-D; and (b), The proper generalization to multidimensions of the discontinuous logical "min" functions used by 1-D schemes is the smooth algebraic form, Eq. 2.1.4, used in the new Vorticity Confinement method.

1. An algebraic nonlinear negative diffusion term similar to that used here was added to a first-order upwind method (which has an implicit positive diffusion) for 1-D passive scalar convection [11]. The result for a constant speed pulse was a convecting, stable solitary wave, spread over a few grid cells. A sequence of amplitudes was plotted for a large number of time steps in a frame moving with the pulse, and it was shown that there was a smooth underlying structure: The sequence of amplitudes at the grid nodes at different time steps was equivalent to that generated by moving the smooth structure through the grid at constant speed and sampling the values on the grid nodes at each time step. The current method appears to give similar results.

2. A more compact method was derived also in [11] where the pulse had support of exactly two grid nodes (two non-zero amplitude values) at each time step. This was actually derived by starting from a Lagrangian particle representation with which it is in 1-1 correspondence, although it was, of course, Eulerian.

3. In the same paper, it was shown that when the scheme was formulated in terms of a new variable,

$$w_i = \sum_0^i u_j$$

where u_i was the original variables. Step functions could be propagated indefinitely. There was a 1-1 correspondence between the two cases.

4. The quantities used in these pulse schemes were first order derivatives of the variables used in the step function schemes. An analog of Vorticity Confinement can be formulated in these 1-D studies by considering the summed variable (w) to be a velocity (v) normal to the 1-D axis (x) and the vorticity the derivative of this along the axis:

$$\omega_1 = \delta_x v(x)$$

We then immediately have a way to generalize to multi-dimensions. Instead of concatenating 1-D operators, we realize that for example, in 2-D incompressible flow there are only 2 rotationally invariant first order derivatives of velocity:

$$D = \vec{\nabla} \cdot \vec{q} \quad ,$$

$$\omega = \vec{\nabla} \times \vec{q} \,|_k$$

where k denotes the direction normal to the 2-D plane.

For incompressible flow, D is, of course, zero and we are led to formulate our multidimensional method only in terms of ω. This is a rational generalization of the 1-D $\delta_x v$ term.

5. The logical "min" function used in the compact 1-D scheme does not seem to be suitable for multidimensions. While not important in 1-D, the field within a 2-D or 3-D feature should be relatively smooth and free of large variations caused by discontinuous logical functions as the feature is rotated. A final generalization, which leads us to our new Vorticity Confinement method, involves the function.

$$\Phi^p = \left[\sum_l \tilde{\phi}_l^{-p} \right]^{\frac{1}{p}}$$

If p is large, $\Phi \rightarrow \min\left\{\tilde{\phi}_l\right\}$. We use p=1 in our method (Eq. 2.1.2), which gives smooth, algebraic results and approximates the "min" function.

6. The discontinuity capturing version of the above 1-D compact pulse scheme (with "min" functions) of Ref. [11] is apparently similar to the recent "superbee" scheme [13].

Appendix II

1

Vorticity Confinement - Recent Results: Turbulent Wake Simulations and A New, Conservative Formulation

J. Steinhoff [1], M. Fan [2], and L. Wang [3]

Abstract

Vorticity Confinement has been shown, over the last several years, to be a way to quickly and cheaply approximate incompressible flows over complex configurations at high Reynolds number. For these flows, there are many important salient features that are reproduced by the method in a simple way, on relatively coarse uniform Eulerian computational grids with fast low-order computational methods. No complex, high order schemes and no extensive refinement or body conforming grid are required. The basic features of the flow that are very effectively simulated all involve vortical regions: thin boundary layers on solid surfaces that are attached or separate, thin vortex sheets and thin filaments that can convect over long distances with no significant physical diffusion, and, finally, turbulent wakes, including small scale effects. These features are very difficult to treat with conventional schemes. The main point is that almost all of the vortical regions in these flows are either thin, so that their internal structure is not important (analogous to shocks or contact discontinuities in compressible flow), or contain small scale structures, such

[1] Professor, The University of Tennessee Space Institute, Tullahoma, TN
[2] Research Scientist, The University of Tennessee Space Institute, Tullahoma, TN
[3] Graduate Research Assistant, The University of Tennessee Space Institute, Tullahoma, TN

Editors: David A. Caughey & Mohamed M. Hafez

as turbulent wakes. All of these vortical structures are, of course, embedded in an incompressible irrotational flow field, which is also efficiently computed.

First, the salient features of Vorticity Confinement solutions will be discussed, to give the reader an understanding of the characteristics of the method. Then, a short presentation of the original formulation of the method will be given and a number of recent papers giving more details referenced. This will be followed by some recent results where the method is used to treat the small scales in turbulent wakes in LES-type simulations. Many other recent results concern free vortices and attached flow over complex configurations, as well as validation studies. Papers describing these will be referred to. Finally, a new, simpler formulation will be described that is effective for both Vorticity Confinement as well as convection of thin streams of passive scalars. Preliminary results of this new formulation for convecting vortices and scalars in 2-D will then be presented.

1.1 Introduction

Vorticity Confinement has been shown, over the last several years, to be a way to quickly and cheaply approximate incompressible flows over complex configurations at high Reynolds number[1–10]. For these flows, there are many important salient features that are reproduced by the method in a simple way, on relatively coarse uniform Eulerian computational grids with fast low-order computational methods. No complex, high order schemes and no extensive refinement or body conforming grid are required. The basic features of the flow that are very effectively simulated all involve vortical regions: thin boundary layers on solid surfaces that are attached or separate, thin vortex sheets and thin filaments that can convect over long distances with no significant physical diffusion, and, finally, turbulent wakes, including small scale effects. These features are very difficult to treat with conventional schemes. The main point is that almost all of the vortical regions in these flows are either thin, so that their internal structure is not important (analogous to shocks or contact discontinuities[11] in compressible flow), or contain small scale structures, such as turbulent wakes. All of these vortical structures are, of course, embedded in an incompressible irrotational flow field, which is also efficiently computed.

The main idea behind Vorticity Confinement is that, at high Reynolds number, the above small vortical scales are modeled on the grid in an inherently discrete, simple way that is much more efficient than if model partial differential equations (pde's) were first formulated and then resolved with finite difference approximations. This modeling involves nonlinear terms in the discrete equations that result in a stable negative total diffusion for the vorticity in a band of length scales. This negative diffusion acts to confine the small scale vorticity to a thickness of about 2 grid cells: Below this scale,

the structure is dominated by a positive diffusion. On scales significantly larger, the negative diffusion causes the structure to contract. The equilibrium solution results from a balance of these two effects. An important feature is that the irrotational flow regions, as well as the very large vortical scales that are present in the turbulent wakes are not significantly affected by these Vorticity Confinement terms and are accurately resolved and convected by the method, which reduces to a conventional CFD method at these large scales.

First, the salient features of Vorticity Confinement solutions will be discussed, to give the reader an understanding of the characteristics of the method. Then, a short presentation of the original formulation of the method will be given and a number of recent papers giving more details referenced. This will be followed by some recent results where the method is used to treat the small scales in turbulent wakes in LES-type simulations[2]. Many other recent results concern free vortices and attached flow over complex configurations, as well as validation studies. Papers describing these will be referred to. Finally, a new, simpler formulation will be described that is effective for both Vorticity Confinement as well as convection of thin streams of passive scalars. Preliminary results of this new formulation for convecting vortices and scalars in 2-D will then be presented[1].

1.2 Vorticity Confinement: Salient Features

There are several different ways to characterize Vorticity Confinement - they are all important in understanding how it works:

1. It is a way of treating flow with small vortical scales as "weak solutions" of the Euler equations, where the small scales are treated as regularized singular regions. In this way it is analogous to shock capturing-quantities are conserved, not at each point but integrated through the vortical feature, which is spread over a few grid cells. The confinement terms serve as a simple implicit model of the internal structure and have little effect on the flow external to the feature, which is accurately treated. Well known examples of this type of treatment include, besides shock capturing, vortex filament and vortex lattice schemes for convecting vortex sheets. Also, the use of panel methods for external flows, where thin vortical boundary layers are simply treated involves similar ideas[12–16]. An important example of this independence of the flow outside the features involves vortex filaments with near-axisymmetric cores with radius of curvature much larger than core radius, where the flow is approximately 2-D in planes normal to the filaments.

2. The current Vorticity Confinement method can be treated as a "zeroth order" approximation for the thin vortical features. As in well-known interacting boundary layer schemes, the basic solution can be treated as a first term in an asymptotic expansion. Higher order terms would involve

modeling some of the effects of the structure, such as displacement thickness and skin friction. In addition to boundary layers, such secondary effects could include long-term spreading of aircraft trailing vortices[17] and modeling of any effects of axial flow on vortex breakdown. For most of the problems that we have treated until now with Vorticity Confinement, these effects have not been very important and the "zeroth order" approach was sufficient. Cases where such higher order effects have already been treated include long-term trailing vortex simulation[17], and a study involving flow separating from a curved surface[3] where the boundary layer was turbulent and affected the separation location.

It should be mentioned that, of course, a very large amount of work has been done, over the last few decades, on turbulent boundary layer modeling using conventional pde-based models, (mostly calibrating Reynolds averaged "RANS" models). The same is true of the small scales in turbulent wakes, using large eddy simulation (LES). By comparison, very little turbulent modeling has been done based on Vorticity Confinement, i.e., by adding "higher order" additional discrete terms with adjustable parameters to the basic method. For these reasons we cannot claim that Vorticity Confinement turbulence models currently exist for these "first order" effects. We are only stating that Vorticity Confinement appears to be a promising approach and a framework for modeling, because of its simplicity and efficiency. Additional work should be done to develop confinement-based turbulence models.

3. For convecting vortex filaments, the internal dynamics is, effectively, treated as "fast" dynamics which approximately satisfies the confinement terms separately from the other, conventional CFD terms used in the method (these will be described below). This fast dynamics is then slaved to the basic fluid dynamics as the filaments are "slowly" convected through the flow.

4. The Vorticity Confinement method can be thought of as incorporating both conventional CFD ideas for solving for the "smooth", large scale features of the flow, and intrinsically discrete ideas for solving for the small scale features: The confinement terms result in intrinsically discrete thin, small scale solitary-wave structures that "live" on the computational lattice. In this way, it is similar to lattice gas approaches. For the large scales, as mentioned, the confinement terms have little effect and the method reverts to conventional CFD, which is well-known to be effective for these scales.

For small scales, the method corrects the well known difficulty of treating thin features (with, of course, large gradients) inherent in conventional CFD schemes. For example, very fine body conforming grids are required with conventional "Navier-Stokes" turbulence modeling methods for boundary layers, and even then, the result is a pde-based *model* solution. Thin boundary layers are very simply treated with confinement as intrinsically discrete structures.

On the other hand, while intrinsically discrete models such as "lattice gas"

can, perhaps, be efficiently formulated for thin regions such as turbulent boundary layers, their treatment of large scales is very inefficient. For example, lattice gas schemes only converge statistically to smooth laminar Navier-stokes solutions; Samples of the solution at large numbers of grid points (N_s), over large numbers of time steps (N_t) must be used in any small region in time and space in order to estimate the solution there. For large scales, therefore, these methods converge like $\sqrt{N_s N_t}$ and can be thought of as "half-order" accurate, as opposed to conventional CFD, for which very high order methods have been developed[18].

1.3 Vorticity Confinement: Basic Formulation

A specific solver will be described which employs Vorticity Confinement. However, Vorticity Confinement can be implemented in a pre-existing flow solver, for both incompressible and compressible flow, by adding a term to the discretized momentum conservation equations[8].

For general unsteady incompressible flows, the governing equations with the Vorticity Confinement term are discretizations of the continuity equation and the momentum equations, with an added term:

$$\nabla \cdot \vec{q} = 0 \qquad 3.0$$

$$\partial_t \vec{q} = -(\vec{q} \cdot \nabla)\vec{q} + \nabla(p/\rho) + [\mu \nabla^2 \vec{q} - \epsilon \vec{s}]h^2/\Delta t$$

where $\vec{q}$ is the velocity vector, p is the pressure, ρ is the density, and μ is a diffusion coefficient that includes numerical effects (we assume physical diffusion is much smaller). For the last term, $\epsilon\vec{s}$, ϵ is a numerical coefficient that, together with μ, controls the size and time scales of the convecting vortical regions or vortical boundary layers. For this reason, we refer to the two terms in the brackets as "confinement terms". Also, h is the grid cell size and Δt the time step.

The first confinement term, or diffusion term is usually specified explicitly, but can be implicitly present in the solver, such as in a lower order upwind scheme. There are also many possible forms for the second confinement term. First, the original one used in this and earlier studies will be described. Then, a new more elegant, simpler form will be described, together with a simple demonstration.

1.4 Original Vorticity Confinement

1.4.1 Formulation

We define the second confinement term as

$$\vec{s} = \frac{1}{h}\hat{n} \times \vec{\omega}$$

where

$$\hat{n} = \frac{\nabla\eta}{|\nabla\eta|}$$

and the vorticity vector is given by

$$\vec{\omega} = \nabla \times \vec{q}$$

and

$$\eta = |\vec{\omega}|$$

In general, for boundary layers and convecting vortex filaments, since computed flow fields *external* to the vortical regions are not very sensitive to the details of the internal structure as long as they are smooth, they are not sensitive to the parameters ϵ and μ over a wide range of values. Hence, the issues involved in setting them are similar to those involved in setting numerical parameters in other analogous computational fluid dynamics schemes, such as artificial dissipation in conventional shock capturing schemes. For wake flows, ϵ and μ can be used to approximately simulate finite Reynolds number effects, since they control the intensity of the small vortical scales. This is an area of study that is just beginning - some results of which will be reported here.

An important feature of the Vorticity Confinement method is that the confinement terms are non-zero only in the vortical regions, since both the first (diffusion) term and the second (anti-diffusion) term vanish outside those regions (care has to be taken in the numerical implementation to preserve this feature).

Another important feature concerns the total change induced by the confinement correction in mass, vorticity and momentum, integrated over a cross section of a convecting vortex. It can be shown[5,9] that mass is conserved because of the pressure projection step in the (incompressible) solver and vorticity is explicitly conserved because of the vanishing of the correction outside the vortical regions. Momentum is almost exactly conserved. An extension of the original method[10] explicitly conserves the momentum at the expense of some additional complications. The new, simpler formulation, described below in Sec.5.2 explicitly conserves momentum with no required extensions.

1.4.2 Results of Wake Study

Two test cases are presented in this section involving the wake structure of a 3-D circular and square cylinder.

1.4.2.1 3-D Circular Cylinder

Flow over a 3-D circular cylinder was calculated to assess the ability of Vorticity Confinement to accurately model the wake flow behind a blunt body. A long cylinder was "immersed" in a uniform $141 \times 101 \times 61$ Cartesian grid in the streamwise, normal and spanwise directions, respectively. Periodic conditions were imposed at the lateral boundaries. The diameter of the cylinder was 15 grid cells. Comparisons between experiment and computed results are given in Figs. 1 and 2. In the figures, the origin of the coordinate system used is located in the center of the cylinder, and all distances are non-dimensionalized by the diameter. The experimental results of Lourenco and Shih[19] at a Reynolds number of about 3,900, were compared to.

The diffusion coefficient μ was held constant for this study. The confinement coefficient, ϵ, was adjusted to impose different levels of confinement. This resulted in different levels of the intensity of the small vortical scales in the wake, and approximately simulated different Reynolds numbers.

Figure 1 depicts the mean streamwise velocities resulting from three values of the confinement coefficient. Figures a) and b) depict the result of two levels of confinement, where the flow is measured along lines traversing the wake (normal to the cylinder axis and the mean stream) at three different locations in the wake of the cylinder. For both values of ϵ the agreement can be seen to be very good, indicating that the effect of the confinement parameter is small over a range of values. Results from a case without confinement ($\epsilon = 0$) are depicted in Fig. 2c. Without confinement, the flow field is dominated by diffusive effects that are not counterbalanced by the anti-diffusive confinement term and approximates a steady, low Reynolds number flow.

The ability of Vorticity Confinement to model the turbulent wake was assessed by computing the rms streamwise velocity fluctuations in the wake region. Comparisons of these fluctuations with the experimental data were made along the same lines in the wake as for the mean velocity, for the same three values of ϵ. Fig. 2a ($\epsilon = 0.25$) shows very good agreement. This is the same value that shows the best agreement for the mean velocity, as can be seen in Fig. 1. The effect of increasing confinement to 0.5 is depicted in Fig. 2b. In general, the effect of increased confinement is to thin the shear layer comprising the wake boundary, and to increase the fluctuation of the time-dependent flow from the mean flow. Fig. 3c depicts results without confinement. Without confinement, the flow can be seen to be steady and exhibits none of the fluctuations that occur when confinement is used.

Figure 3 depicts isosurfaces of vorticity magnitude for the same three levels of confinement. The use of confinement results in chaotic flow patterns, as would be expected in three-dimensional turbulent flows. This does not occur in two-dimensional simulations, indicating that this chaotic behavior is not due to numerical instability created by the confinement. Increasing confinement increases the chaotic nature of the flow in 3-D and reduces the characteristic size of the vortical structures, analogous to what would be expected with an increase in Reynolds number. Clearly, the use of confinement allows small-scale time-dependent wake structures to be generated on extremely coarse grids with the small-scale structure captured over only $1 \sim 2$ grid cells. Also, these small-scale structures serve as a viscous sink for turbulent energy, as in physical turbulence.

1.4.2.2 3-D Square Cylinder

Flow over a square cylinder was also calculated. As in the circular case, the cylinder was "immersed" in a uniform $141 \times 101 \times 61$ Cartesian grid and periodic conditions imposed at the lateral boundaries. The diameter (length of each side) of the cylinder was also 15 grid cells. The same coordinate system was used as for the circular cylinder. Results of the computations were compared to the experimental results of Lyn et al.[20] at a Reynolds number of about 21,400.

As in the circular cylinder case, the diffusion coefficient μ was set to 0.15. The confinement coefficient, ϵ, was adjusted to impose different levels of confinement so as to approximate the effects of different Reynolds numbers.

Figure 4 depicts the comparison with experimental data of the time-averaged streamwise velocity along a streamwise line extending downstream from the middle of the leeward face of the cylinder. Results of two values of the confinement coefficient are plotted. Figure 6 shows the time-averaged velocity along a line traversing the wake (normal to the cylinder axis and the mean stream), as in the circular case, at $x = 1$. Symbols represent the experimental data. Our numerical results agree well with the experimental data for $\epsilon = 0.35$ and $\epsilon = 0.25$.

Comparisons of the computed turbulence level with the experimental results also show reasonably good agreement in Fig. 6a. As in the circular case, the same value of ϵ that gave good agreement with experiment for RMS velocity also gave good agreement formean velocity. The effect of decreasing confinement is shown in Fig. 6b. Comparing this case with the previous 3-D circular cylinder case, it is easy to see that a higher value of ϵ is required for better results. This is apparently because the Reynolds number has increased from about 3,900 in the 3-D circular cylinder case to roughly 21,400 in the present 3-D square cylinder case.

1.4.2.3 Synopsis of Cylinder Study

In subsequent studies, the correlation between ϵ and Reynolds number will be studied by comparisons between computation and experiment for other cases and a useful calibration of ϵ determined. Also, it should be emphasized that our agreement with experiment is closer than many much finer, conforming grid studies with much more complex LES pde models[21], each requiring a number of empirical coefficients. As explained, just one coefficient is adjusted here, on a simple, coarse uniform Cartesian grid.

1.5 New Vorticity Confinement

1.5.1 Formulation

Because additional corrections must be added to make the original confinement explicitly conserve momentum, a new, simpler formulation that does not have these problems has been developed. This new, intrinsically discrete formulation is presented in this section.

A more detailed description is presented in [1]. First, a formulation for scalar confinement is given. Then, a velocity-based (primitive variable) Vorticity Confinement correction is given that reduces to the scalar confinement in terms of vorticity when the curl is taken.

1.5.1.1 Scalar Formulation

The scalar formulation presented here is related to that presented in [8] in 1-D.

We start with the form for a scalar :

$$\phi^{n+1} = \phi^n - \Delta t \nabla \cdot \vec{q}\phi^n + \delta\phi^n \qquad 5.1.1$$

where the confinement correction:

$$\delta\phi^n = h^2[\mu\nabla^2\phi^n - \epsilon\nabla^2\Phi^n]$$

where

$$\Phi^n = \left[\frac{\sum_l C_l(\phi^n + \delta)^{-1}}{\sum_l C_l}\right]^{-1} \qquad 5.1.2$$

where the sum is over a set of grid nodes near and including the node where Φ is computed, and δ is a small positive constant ($\sim 10^{-8}$) to prevent problems due to finite precision. The coefficients, C_l, can be varied but good results are

obtained by simply setting them to 1. For example, in 2-D, one possibility is

$$\Phi_{ij}^n = \left[\frac{\sum_{\alpha=-1}^{+1} \sum_{\beta=-1}^{+1} (\phi_{i+\alpha,j+\beta}^n + \delta)^{-1}}{N} \right]^{-1} \qquad 5.1.3$$

where N neighboring terms are taken.

Here, we assume $\phi^n \geq 0$. Negative values can also be accommodated with a small extension. Both μ and ϵ are positive.

An important feature is that all terms are homogeneous of degree 1 in Eq. 5.1.1. This is important because the confinement not depend on the scale of the quantity being confined. Another important feature is the nonlinearity. It is easy to show that a linear combination of terms of different order in the derivatives cannot lead to a stable confinement for any finite range of coefficients.

For smooth ϕ fields (large scales), the last term represents a negative diffusion. If $\mu \leq \epsilon$, where N is the number of terms in Eq. 5.1.2, the total diffusion is negative. However, the iteration of Eq. 5.1.1 is still stable and converges for values of ϵ up to about 5μ, resulting in an effective negative diffusion coefficient in the long wavelength limit. Also, for $\vec{q} = 0$, the discrete, converged solution can be given exactly in terms of (translationally invariant) sech functions.

For convection using a conservative discretization, the total amplitude

$$< \Phi > \equiv \sum_{ij} \phi_{ij}^n$$

is independent of n. If we define the centroid of an isolated region,

$$< \vec{X} >^n \equiv \sum_{ij} \vec{x}_{ij}^n \phi_{ij}^n / < \Phi >$$

and the weighted mean velocity

$$< \vec{Q} >^n \equiv \sum_{ij} \vec{q}_{ij}^n \phi_{ij}^n / < \Phi >$$

where $\vec{x}_{ij}$ is the (fixed) position vector of node (i, j), and ϕ_{ij} and $\vec{q}_{ij}$ are the scalar value and the velocity at that node, then the centroid evolves according to:

$$< \vec{X} >^{n+1} = < \vec{X} >^n + \Delta t < \vec{Q} >^n$$

For vortices, the self-induced velocity which is included in the above sum exactly cancels and, as in the passive scalar case, the $\vec{q}_{ij}$ can be taken to be an externally applied (irrotational) velocity. The above result then still holds.

Since we are, at this point, only interested in the "expectation values" of scalars or vorticities for thin features and that the features remain compact, spread over only a few cells, this Ehrenfest-type relation is exactly what we need. Only the variables of importance are, effectively, solved for. This shows that the features, when isolated, evolve as particles with essentially no internal dynamics. However, we keep the very important Eulerian feature that the number of features is not fixed. We could, for example, create additional solitary waves by inserting a source: No additional computational markers need be created, as in Lagrangian schemes. For this study, we show that features can automatically merge and reduce in number. This will be seen in the results of Sec. 5.2. As for the earlier Vorticity Confinement method, this property is crucial for the general treatment of interacting vortical regions, especially in 3-D[4,7,9,10].

1.5.1.2 Vorticity Formulation

The next step involves letting ϕ be the magnitude of vorticity and deriving an equation for the corresponding velocity correction that leads to Eq. 5.1.1 when the curl is taken (in 2-D). This correspondence is still close for a 3-D vortex filament if the radius of curvature is large so that the flow is approximately 2-D in sections normal to the filament axis. This will result in a new formulation of Vorticity Confinement.

We simply define

$$\vec{q}^{n+1} = \vec{q}^n + \Delta t \nabla \cdot \vec{q}^n q^n + \delta \vec{q}^n \qquad 5.1.4$$

where the confinement correction:

$$\delta \vec{q}^n = h^2(\mu \nabla^2 \vec{q}^n + \epsilon \nabla \times \vec{w}^n)$$

or, for $\nabla \cdot \vec{q}^n = 0$,

$$\delta \vec{q}^n = -h^2 \nabla \times (\mu \vec{\omega}^n - \epsilon \vec{w}^n)$$

where

$$\vec{\omega}^n = \nabla \times \vec{q}^n$$

and

$$\vec{w}^n = \frac{\vec{\omega}^n}{|\vec{\omega}^n| + \delta} \left[\frac{\sum_l (|\vec{\omega}_l^n| + \delta)^{-1}}{N} \right]^{-1} \qquad 5.1.5$$

where the sum is the same as in Eq. 5.1.3.

1.5.2 Results

All results presented are in 2-D. Also, all convection cases use a conservative second-order centered convection term together with a centered diffusion term and are first-order-explicit in time. In all the result plots, axes are labeled with grid node location. Plots of amplitude are made using dense contours with white grid lines superimposed.

1.5.2.1 Passive Scalar Convection

A good test involves convection of a small passive scalar pulse in solid-body rotating flow[22]. For this case a convection step was followed by a single confinement step (including diffusion). The full summation of Eq. 5.1.2 with $C_l = 1$ (Eq. 5.1.3) leads to a spreading of the pulses in the direction normal to their motion (This spreading does not occur for vortices, for reasons described in Sec. 5.2.2). This scalar spreading seemed to be due to the inclusion of "downwind" values, which is known to cause instability. By setting $C_l = 0$ for downwind points, the problem is almost completely cured, and only a very weak spreading remains.

Results are shown in Fig. 7a for a single pulse convecting through the 1st rotation (2π) and in Fig. 7b through the 10th rotation. Contours are plotted from initial maximum value to 1/3 of that value. The final image in Fig. 7b was after 12,560 time steps. This represented a travel of 1,256 cells or about 433 pulse diameters. The open circle labels the starting location. The time step was not set to exactly divide the circuit so we would not expect the final image to exactly coincide with the initial one. However, the final position is within plottable accuracy of the calculated angle and radius. The final radius can be seen to be very close to the initial one. This is somewhat surprising since the method was only first order in time and second order in space. We have not yet attempted to reduce the small, residual cross-flow spreading. This could easily be accomplished with a small amount of additional negative diffusion in the cross-stream direction. For the case computed, we used $\mu = 0.15$ and $\epsilon = 0.75$.

Finally, a run was made with no confinement and a lower, (minimal) diffusion set for stability. The maximum amplitude decreased to below the plotting threshold after only $\pi/8$ radians of travel (position of the first image in Fig. 2a).

1.5.2.2 Vorticity Convection

The incompressible fluid dynamic equations with Vorticity Confinement, Eq. 3.0, were discretized and solved. Each time step, the same convection scheme used for the above scalar was used. A standard pressure projection

method was used to enforce incompressibility[23]. This used a staggered grid for pressure and velocity and a box scheme for the pressure gradient. The required Poisson equation for pressure was solved using a direct method "FishPack". Vorticity Confinement terms - Eqs 5.1.4 and 5.1.5, were used, with $\mu = 0.05$ and $\epsilon = 1.5\mu$. Results were very close to those for $\mu = 0.2$ and $\epsilon = 1.5\mu$, implying that the method is not very sensitive to the values of these parameters. (Further investigation of this point should be done). The time step, based on grid cell size and circumferential velocity near the vortex cores, was 0.4 and the grid had 128×128 cells. For vortices, the full summation (Eq. 5.1.3) with all $C_l = 1$ was used, without excluding downwind points. This exclusion, useful for scalar convection, was not important here because the large circulating velocities near the vortex cores rapidly convected any cross-stream spread vorticity around the cores, keeping them close to axisymmetric. The confinement then kept the cores compact.

First, interacting vortices of opposite sign were computed with no external free-stream-velocity, convecting only under their own induced velocities. To approximate far-field boundary conditions, each time step the total amplitudes and centroids of both positive and negative vorticity were computed. The velocities induced by corresponding point vortices at these locations were computed and imposed on the boundaries. Dirichlet conditions were used for pressure.

Results are presented in Fig. 8 for a sequence of time steps. The computed vortex centroids are convecting at the same velocity, to plottable accuracy, as if they were point vortices. The self-induced velocity in each vortex, although several times the convecting velocity of the centroid, automatically cancels and has no effect because the method conserves momentum, as explained in Sec. 5.1.1. The final images shown result from 1,800 time steps, yet the vortices are just as compact as initially. It should be mentioned that if the vortices are significantly closer, there will be an interaction and eventually vorticity will be exchanged. This is to be expected since there are "tails" of vorticity that (rapidly) decrease with radius beyond the region shown.

Vortices with the same sign were computed as they rotated around each other under their induced velocities. The vortices were initially (and finally) separated by 14 cells. First, the computation was done with no Vorticity Confinement, and with minimum diffusion required for convective stability. Contours are displayed in Fig. 9 corresponding to vorticity values between initial maximum and 1/4 of that value. It can be seen that the vorticity rapidly

diffuses. The computation was repeated with Vorticity Confinement. Values of μ and ϵ were those used above for opposite sign vortices. Vorticity contours between initial maximum and 1/4 maximum are displayed for 3 different times in the 1st loop around each other in Fig. 9a, and in the 20th loop in Fig. 9b. The behavior is as expected: The vortices can be seen to be essentially the same at the end (after 7,200 time steps) as initially.

As stated, the main reason for using an Eulerian method as opposed to Lagrangian is to allow vortices to merge and otherwise change topology, so that complex, realistic vortical configurations can be treated. This has been amply demonstrated by the original Vorticity Confinement method both in 2-D and 3-D[4,5,7,9,10]. To demonstrate that the new confinement method does not inhibit this merging we repeat the above computation, but with the vortices initially 5 cells apart. This is a repeat of a calculation using the original Vorticity Confinement method[5]. It is known from vorticity contour of "waterbag" methods[24] that corotating vortices become unstable and merge when they are initially closer than a few diameters. It can be seen in the vorticity contour plots of Fig. 10 that this merging automatically occurs, as expected, with the new Vorticity Confinement method.

1.6 Conclusion

The ability of the original Vorticity Confinement method to efficiently compute blunt body turbulent wakes was demonstrated. This involved an LES-type representation but with the small scales treated as inherently discrete structures. The computations involved a circular and square cylinder in 3-D.

A new Eulerian Vorticity Confinement has been introduced. Its advantages over the original Vorticity Confinement method are that it is simpler and easier to analyse and explicitly conserves total momentum. The method accurately convects thin features, either vortices or scalars, over very long distances, even though they are confined to only 2-3 grid cells. As in shock and other discontinuity capturing schemes, the details of the internal structure of the feature are not solved for, but implicitly modeled (the features are treated as weak solutions). Integral quantities, such as total amplitude and centroid, however, are accurately solved for. As such, the method essentially represents the features as nonlinear discrete solitary waves that live on the computational lattice. It is argued that the new method is a rational generalization of 1-D discontinuity confinement schemes to multiple dimensions.

Examples are presented for thin, convecting passive scalars and vortices in 2-D incompressible flow.

Acknowledgements

The first author acknowledges many helpful discussion with Barry Merriman and Stanley Osher. The work was supported by the Army Research Office and the University of Tennessee Space Institute.

REFERENCES

1. Steinhoff, J., Fan, M., and Wang L., "Convection of Concentrated Vortices and Passive Scalars As Solitary Waves", submitted to *Journal of Scientific Computing*, May, 2002.
2. Fan, M., Wenren, Y., Dietz, W., Xiao, M., Steinhoff, J., "Computing Blunt Body Flows On Coarse Grids Using Vorticity Confinement", to appear in *Journal of Fluids Engineering*, December, 2002.
3. Wenren,Y., Fan, M., Dietz, W., Hu, G., Braun, C., Steinhoff, J., and Grossman, B., "Efficient Eulerian Computation of Realistic Rotorcraft Flows Using Vorticity Confinement", AIAA-01-0996 (2001).
4. Steinhoff, J., Wenren, Y., Braun, C., Wang, L., and Fan, M. "Application of Vorticity Confinement to the Prediction of the Flow over Complex Bodies", pp. 197-226 in *Frontiers of Computational Fluid Dynamics 2002* (D.A. Caughey and M.M. Hafez eds.); World Scientific, (2002)
5. Steinhoff, J., Mersch, T., and Wenren, Y., "Computational Vorticity Confinement: Two Dimensional Incompressible Flow", Proceedings of the Sixteenth Southeastern Conference on Theoretical and Applied Mechanics. 1992.
6. Steinhoff, J., Wang, Clin, Underhill, D., Mersch, T., and Wenren, Y., "Computational Vorticity Confinement: A Non-Diffusive Eulerian Method for Vortex-Dominated Flows," UTSI preprint, 1992.
7. Steinhoff, J., "Vorticity Confinement: A New Technique for Computing Vortex Dominated Flows," In D.A. Caughey and M.M. Hafez, editors,*Frontiers of Computational Fluid Dynamics.* John Wiley & Sons, 1994.
8. Steinhoff, J., Puskas, E., Babu, S., Wenren, Y., and Underhill, D., "Computation of Thin Features Over Long Distances Using Solitary Waves," AIAA Proceedings, 13th Computational Fluid Dynamics Conference, July, 1997.
9. Steinhoff, J. and Underhill, D., "Modification of the Euler Equations for Vorticity Confinement Application to the Computation of Interacting Vortex Rings", *Physics of Fluids*, 6, 1994.
10. Wenren, Y., Steinhoff, J., Wang, L., Fan, M., and Xiao, M., "Application of Vorticity Confinement to the Prediction of the Flow over Complex Bodies," AIAA Paper No. 2000-2621, Fluids 2000, Denver, CO, June, 2000.
11. Harten, A., "The Artificial Compression Method for Computation of Shocks and Contact Discontinuities III, Self-Adjusting Hybrid Schemes", *Mathematics of Computation*, Vol. 32, No. 142. April 1978.
12. Hoeijmakers, W.M., and Vaatstra, W., "A Higher Order Panel Method Applied to Vortex Sheet Roll-Up", *AIAA Journal*, Vol.21, 1983.
13. Rosenhead, *Proc. Roy. Soc., A, 134*, 1931, p.170.
14. Westwater, *Reports and Memoranda, 1692*, 1936.
15. R. Krasny, "Vortex Sheet Computations: Roll-Up, Wakes, Separation", *Lectures in Applied Mathematics, 28*, 1991.
16. A. Leonard, "Vortex Methods for Flow Simulation", *J. Comput. Phys., 37*, 289

(1980).
17. Steinhoff, J., and Wenren, Y., "Computation of Generation and Convection of Aircraft Vortices", NASA SBIR Contract NAS1-97068 Final Report, Flow Analysis Inc., 1997.
18. Hirsch, C., *Numerical Computation of Internal and External Flows*, John Wiley & Sons, 1990.
19. Ma, X., Karamanos, G., and Karniadakis, G., "Dynamics and Low-Dimensionality of a Turbulent Near Wake," *J. Fluid Mech.*, 410, pp. 29-65, 2000.
20. Lyn, D.A., Einav, S., Rodi, W., and Park, J.H., "A Laser-Doppler Velocimetry Study of Ensemble-Averaged Characteristics of the Turbulent Near Wake of a Square Cylinder ", *J. Fluid Mech.*, 304, pp. 285-319, 1995.
21. Rodi, W., "Large-Eddy Simulation and Statistical Turbulence Models: Complementary Approaches", *New Tools In Turbulence Modeling*, Eds. Metais, O. and Ferziger, J.. Springer-Verlag 1997.
22. Orszag, S.A., "Numerical Simulation of Incompressible Flows Within simple Boundaries: Accuracy", *J. Fluid Mech.*, 49, 1971.
23. Kim, J., and Moin, P., "Application of a Fractional Step Method to Incompressible Navier-Stokes Equations", *Journal of Computational Physics*, Vol. 59, 1995.
24. Overman, E.A. and Zabusky, N.J., "Evolution and Merger of Isolated Vortex Structures", *Journal of Physical Fluids*, Vol. 25, 1982.

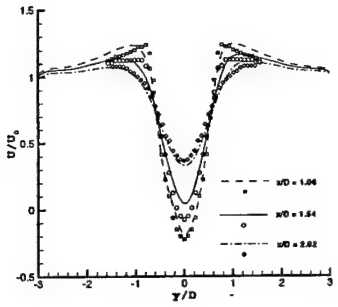

(a) $\mu = 0.15, \epsilon = 0.25$

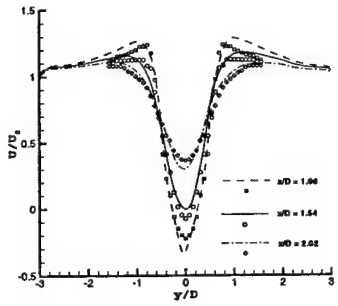

(b) $\mu = 0.15, \epsilon = 0.5$

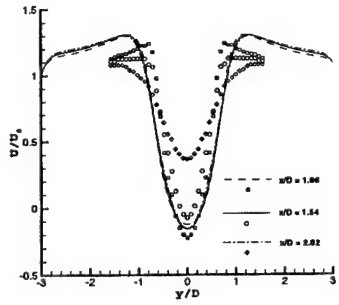

(c) $\mu = 0.15, \epsilon = 0.$ (No Confinement)

Figure 1 Mean Streamwise Velocity Profiles

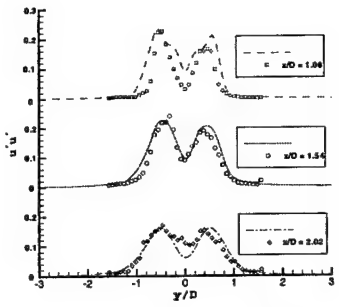

(a) $\mu = 0.15, \epsilon = 0.25$

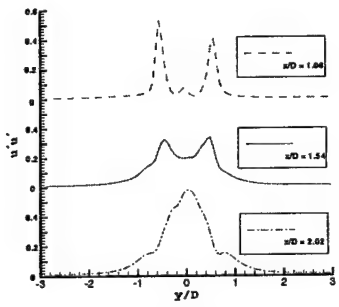

(b) $\mu = 0.15, \epsilon = 0.5$

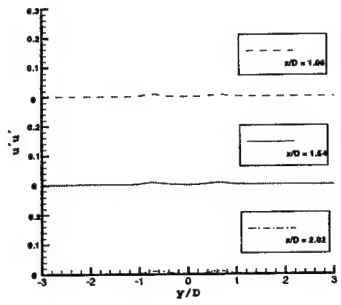

(c) $\mu = 0.15, \epsilon = 0.$ (No Confinement)

Figure 2 Streamwise RMS Fluctuations

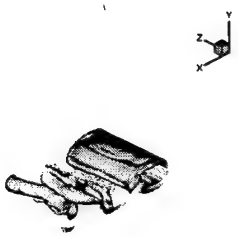

(a) $\mu = 0.15, \epsilon = 0.25$

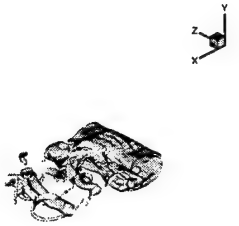

(b) $\mu = 0.15, \epsilon = 0.5$

(c) $\mu = 0.15, \epsilon = 0.0$ (No Confinement)

Figure 3 Isosurfaces of Vorticity Magnitude (Isosurface Level = 0.15)

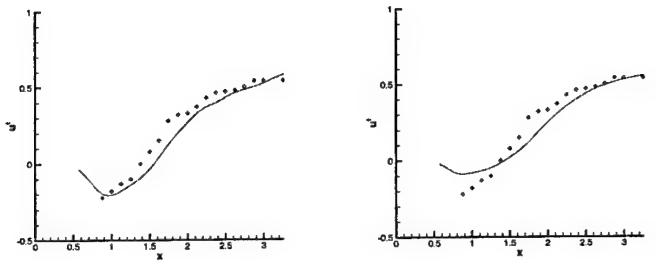

(a) $\epsilon = 0.35$ (b) $\epsilon = 0.25$

Figure 4 Comparison of time-averaged streamwise velocity along a streamwise line. Symbols denote experimental data.

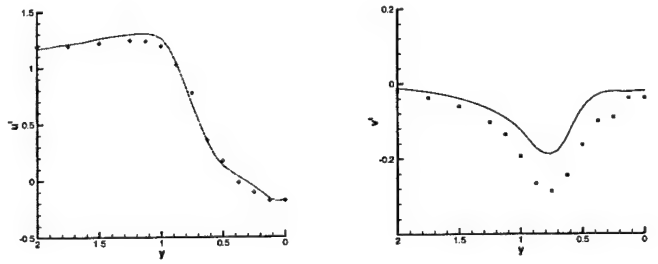

(a) $\epsilon = 0.35$

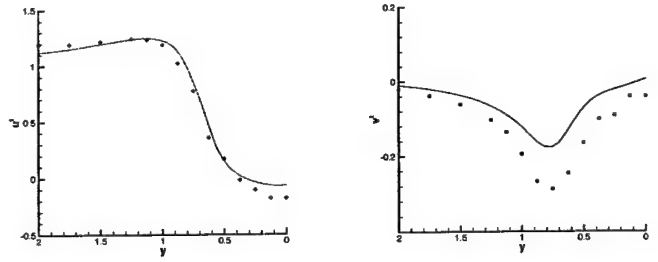

(b) $\epsilon = 0.25$

Figure 5 Comparison of time-averaged velocity profiles at x = 1. Symbols are experimental data.

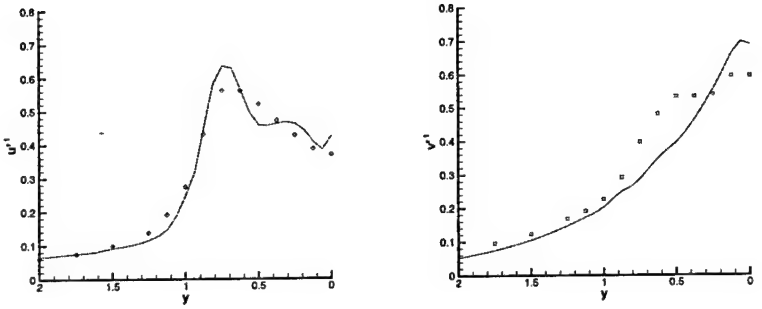

(a) $\epsilon = 0.35$

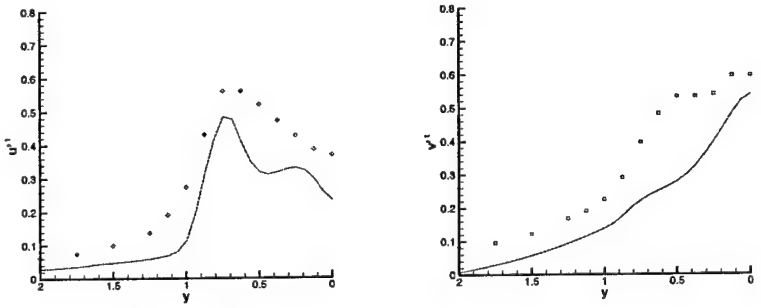

(b) $\epsilon = 0.25$

Figure 6 Comparison of root mean square velocity fluctuation profiles at x = 1. Symbols are experimental data.

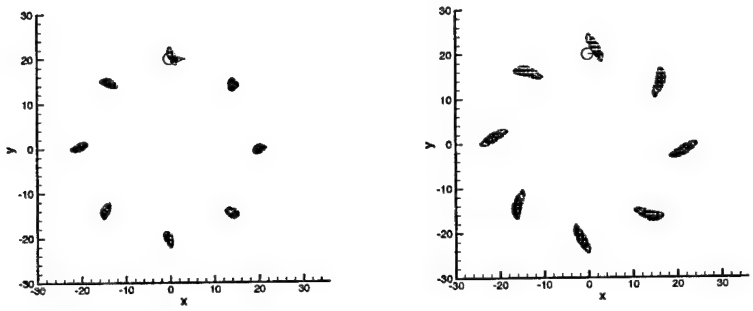

(a) 1st loop (b) 10th loop

Figure 7 Scalar convection

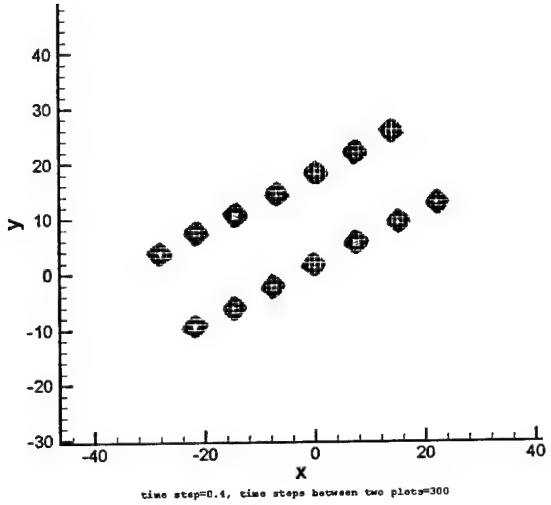

Figure 8 Vorticity contour plots of self-induced flow by two point vortices (15 cells apart) with opposite sign

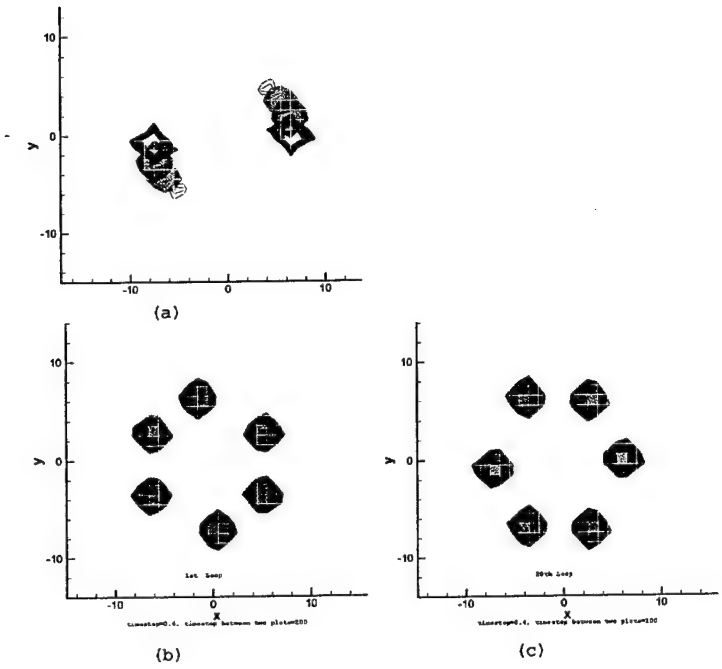

Figure 9 Vorticity contour plots of self-induced flow by two vortices (14 cells apart) with same sign. (a) without Vorticity Confinement; (b)with Vorticity Confinement, 1st loop; (c)with Vorticity Confinement, after 20th loops.

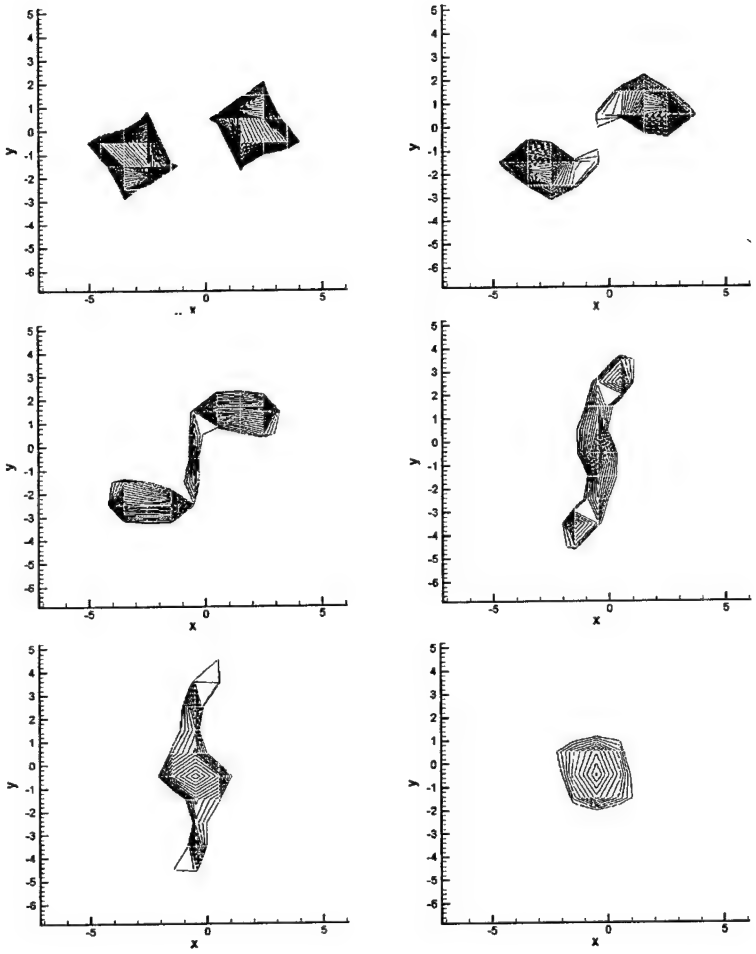

Figure 10 Vorticity contour plots of self-induced flow by two vortices (5 cells apart) with same sign, with Vorticity Confinement

Appendix III

COMPUTING BLUNT BODY FLOWS ON COARSE GRIDS USING VORTICITY CONFINEMENT

M. Fan §, Y. Wenren +, W. Dietz +, M. Xiao§, J. Steinhoff §

§ University of Tennessee Space Institute, Tullahoma, TN
+ Flow Analysis, Inc., Tullahoma, TN

To be Published, ASME Journal of Fluids Engineering, December, 2002

Abstract

Over the last few years, a new flow computational methodology, Vorticity Confinement, has been shown to be very effective in treating concentrated vortical regions. These include thin vortex filaments which can be numerically convected over arbitrary distances on coarse Eulerian grids while requiring only ~2 grid cells across their cross section. They also include boundary layers on surfaces "immersed" in non-conforming uniform Cartesian grids, with no requirement for grid refinement or complex logic near the surface.

In this paper we use Vorticity Confinement to treat flow over blunt bodies, including attached and separating boundary layers, and resulting turbulent wakes. The same basic idea is applied to all of these features: At the smallest scales (~2 cells) the vortical structures are captured and treated, effectively, as solitary waves that are solutions of nonlinear discrete equations on the grid. These do not represent discretizations of partial differential equations (pde's) but nonlinear models of the structures, directly on the grid. They allow the boundary layer to be effectively "captured". In the turbulent wake, where there are many scales, they represent an effective small scale energy sink. However, they do not have the unphysical spreading due to numerical diffusion at these scales, which is present in conventional computational methods.

The basic modeling idea is similar to that used in shock capturing, where intrinsically discrete equations are satisfied in thin, modeled regions. It is argued that, for realistic high Reynolds number flows, this direct, grid-based modeling approach is much more effective than first formulating model pde's for the small scale, turbulent vortical regions and then discretizing them.

Results are presented for 3-D flows over round and square cylinders and a realistic helicopter landing ship. Comparisons with experimental data are given.

Finally, a new simpler formulation of Vorticity Confinement is given together with a related formulation for confinement of passive scalar fields.

1. Introduction

Many real-world flows are characterized by regions of concentrated vorticity. These are typically turbulent at realistic Reynolds numbers and can convect over long distances, either as thin vortex filaments or blunt body wakes containing small-scale vortical structures. Also, boundary layers are typically thin, turbulent vortical structures near solid surfaces. Even though the Navier-Stokes equations apply to these flows, it is not feasible to solve them on foreseeable computers due to the ever-present small scales. As a result, conventional CFD methods involve first formulating the partial differential equations (pde's) that model these turbulent regions. These pde's are then discretized in the turbulent regions and then solved. This typically requires large computer resources and difficult grid generation. The problem is that resolving even the model pde's requires very fine computational grids, which must conform to the surface for the boundary layer. Further, these methods typically dissipate thin filaments and vortical structures in the wake as they convect. This is true even if on the order of 10 grid points are devoted to the cross section of each structure and complex, high order discretizations are used. The problem is intrinsic to the discretization of the convective terms and made worse by the use of dissipative terms to model the turbulent effects. Finally, even if the model pde's *are* resolved, the result is, of course, still a model approximation of the turbulent flow.

In this paper, we describe an entirely new CFD methodology where very different numerical models are used for vortical regions. Instead of first hypothesizing a turbulence model based on pde's and then trying to accurately discretize and resolve them, we model the internal structure of the vortical regions *directly* on the grid using generalized nonlinear *difference* equations, rather than using finite difference discretizations of partial differential equations that attempt to approximately resolve the model equations (and the vortical structures). This approach allows treatment of vortical structures as objects spread over only 1-2 grid cells on coarse, essentially uniform Cartesian computational grids.

These ideas are implemented in the methodology termed ***Vorticity Confinement***. Although new for vortical regions, these ideas are old for the treatment of shocks, starting with VonNeumann & Richtmyer [1], Lax [2] and others. There, as is well known, shocks are treated as thin regions spread over a few grid cells that obey discrete, grid-based nonlinear model equations, that conserve certain quantities. This approach has been shown to be more effective than trying to discretize and solve the applicable Navier-Stokes pde's in those thin regions. One difference, however, is that with shocks, unlike vortical regions, characteristics slope inward toward the shock. As a result, the modeling is simpler than that with vortical structures. One of the first confinement-type schemes for contact discontinuities, where, unlike shocks, physical characteristics do not help, was

developed by Harten [3], but was specialized to one-dimensional compressible flow.

Many results have been obtained in recent years using Vorticity Confinement [4-22]. Lohner has a very good short review of this work [18]. Initial results were for isolated, convecting vortex filaments [14-16]. Then, vortices convecting past airfoils and wings (blade – vortex interactions) were treated [13]. In this early study, unlike in our current studies, near the surface a surface-fitted grid was used for the wing with surface grid refinement to resolve the actual Navier-Stokes equations, since only a low Reynolds number, laminar, case was treated. To accommodate this grid refinement with Vorticity Confinement, the parameter specifying the strength of the Vorticity Confinement term (ε) was made to be proportional to grid size so that it automatically vanished in the fine-grid boundary layer region, but was able to confine the convecting vortex in the external, coarse-grid region. Our current studies, like those described in this paper, involve surfaces "immersed" in uniform, non-conforming grids with no grid refinement and use a constant value for ε.

Recently, Vorticity Confinement has been used together with unstructured grids [18, 19]. When using these grids, which have rapidly changing cell sizes, care must be taken not only that ε varies properly with cell size, but also that the confinement correction does not extend beyond the vortex core due to numerical artifacts of the implementation. This property is true in the continuum limit, as shown in the description of Sec.2, and should be preserved in the discretization. If the correction *does* extend beyond the vortex, then it could erroneously affect surface pressure if a vortex is passing near a surface. This could be important, for example, for delta wings [18] and similar cases, where vortices convect near surfaces. In fact, for delta wings, it is well known that there is a feeding sheet from the leading edge causing the vortex to grow in strength as it convects and causing the characteristics to point towards it. In such cases, for a reasonable grid, confinement is not really needed (until the vortex convects past the trailing edge). If confinement is used correctly, however, it should not change the nearby pressure on the surface even in these cases, for high Reynolds number flow. Finally, in low Reynolds number viscous flow cases where laminar flow occurs, the proper Navier-Stokes equations should, of course, be used, since the vortical scales are then not small and there is no need to discretize model equations for small scales.

In this paper, Vorticity Confinement is applied to a series of blunt bodies, a circular and a square cylinder, and a realistic helicopter landing ship. In the cylinder cases, for which unsteady experimental results are available, comparison is made. The ship case demonstrates the ability of Vorticity Confinement to preserve thin, concentrated vortical structures over long distances. Also velocity and vortex trajectory computations are shown to agree well with experimental results. All cases were run on grids much coarser than those required by conventional CFD methods and did not require body conforming grid generation or refinement near the surfaces.

2. Vorticity Confinement

Vorticity Confinement is a method to preserve convecting, concentrated vorticity on a coarse grid; the vortical structures can represent boundary layers over solid surfaces, the smaller scales (of the order of a grid cell) in turbulent wakes, or separated, thin vortex filaments that convect over arbitrarily long distances. Vorticity Confinement can be implemented in a pre-existing flow solver, for both incompressible and compressible flow, by adding a term to the discretized momentum conservation equations [12].

For general unsteady incompressible flows, the governing equations with the Vorticity Confinement term are discretizations of the continuity equation and the momentum equations, with an added term:

$$\nabla \cdot \vec{q} = 0 \qquad 2.0.1$$

$$\partial_t \vec{q} = -(\vec{q} \cdot \nabla)\vec{q} - \frac{1}{\rho}\nabla p + [\mu \nabla^2 \vec{q} - \varepsilon \vec{s}] \qquad 2.0.2$$

where $\vec{q}$ is the velocity vector, p is the pressure, ρ is the density, and μ is a diffusion coefficient that includes numerical effects (we assume physical diffusion is much smaller). For the last term, $\varepsilon\vec{s}$, ε is a numerical coefficient that, together with μ, controls the size and time scales of the convecting vortical regions or vortical boundary layers. For this reason, we refer to the two terms in the brackets as "confinement terms".

The first confinement term, or diffusion term is usually specified explicitly, but can be implicitly present in the solver, such as in a lower order upwind scheme. There are also many possible forms for the second confinement term. First, the original one used in this and earlier studies will be described. Then, a new more elegant, simpler form will be described, together with a simple demonstration.

2.1 Original Form

$$\vec{s} = \hat{n} \times \vec{\omega} \qquad 2.1.1$$

where

$$\hat{n} = \nabla\eta / |\nabla\eta| \qquad 2.1.2$$

the vorticity vector is given by

$$\vec{\omega} = \nabla \times \vec{q} \qquad 2.1.3$$

and

$$\eta = |\vec{\omega}| \qquad 2.1.4$$

In general, for boundary layers and convecting vortex filaments, computed flow fields *external* to the vortical regions are not sensitive to the parameters ε and μ over a wide range of values. For example, the flow outside an axisymmetric 2-D vortex core is independent of the vortical distribution, and hence does not depend on ε and μ as long as the core is thin. Hence, the issues involved in setting them are similar to those involved in setting numerical parameters in other standard computational fluid dynamics schemes, such as artificial dissipation in many conventional compressible solvers. There, the flow outside 1-D captured shock regions does not depend on the exact internal structure, as long as it is

thin. For wake flows, ε and μ can be used to approximately simulate finite Reynolds number effects, since they control the intensity of the small vortical scales.

An important feature of the Vorticity Confinement method is that the Confinement terms are non-zero only in the vortical regions, since both the diffusion term and the anti-diffusion term vanish outside those regions (care has to be taken in the numerical implementation to preserve this feature).

Another important feature concerns the total change induced by the confinement correction in mass, vorticity and momentum, integrated over a cross section of a convecting vortex. It can be shown [14,16] that mass is conserved because of the pressure projection step in the solver and vorticity is explicitly conserved because of the vanishing of the correction outside the vortical regions. Momentum is almost exactly conserved. A small extension of the original method [9], explicitly conserves the momentum. The new formulation, described below in Sec.2.2 also explicitly conserves momentum.

It should be mentioned that the above pde form for the confinement cannot be said to be resolved since vorticies are captured in only a few grid cells. Accordingly, we can only say that the pde form is only used to *motivate* the final discrete form and that a large body of numerical evidence has been given that the terms result in confined vortices.

2.2 New Vorticity Confinement Formulation

Because of the above issue concerning the pde form and that additional corrections must be added to make it explicitly conserve momentum, a new, simpler formulation that does not have these problems has been developed. This new, intrinsically discrete formulation is presented in this section.

A more detailed description is being presented in [23]. First, a formulation for scalar confinement is given. Then, a velocity-based Vorticity Confinement correction is given that reduces to the scalar confinement in terms of vorticity when the curl is taken.

The scalar formulation presented here is related to that presented in [12] in 1-D. In this section no convection is used, only the two confinement terms, so that the behavior can be seen more clearly. Excellent results are found with convection and will be shown in [23].

We start with an iteration for a scalar ϕ :

$$\phi^{n+1} = \phi^n + \mu\nabla^2\phi^n - \varepsilon\nabla^2\Phi^n \quad 2.2.1$$

where

$$\Phi^n = \left[\frac{\sum_l C_l\left(\phi_l^n + \delta\right)^{-1}}{\sum_l C_l}\right]^{-1} \quad 2.2.2$$

where the sum is over a set of grid nodes near and including the node where Φ is computed, and δ is a small positive constant ($\sim 10^{-8}$) to prevent problems due to finite precision. The coefficients, C_l, can be varied but good results are obtained by simply setting them to 1.

For example, in 2-D, one possibility is

$$\Phi_{ij}^{n} = \left[\frac{\sum_{\alpha=-1}^{+1} \sum_{\beta=-1}^{+1} \left(\phi_{i+\alpha, j+\beta} + \delta \right)^{-1}}{N} \right]^{-1} \qquad 2.2.3$$

where N neighboring terms are taken.

Here, we assume $\phi^n \geq 0$. Negative values can also be accommodated with a small extension. Both μ and ε are positive.

An important feature is that all terms are homogeneous of degree 1 in Eq. 2.2.1. This is important because the confinement not depend on the scale of the quantity being confined. Another important feature is the nonlinearity of different order in the derivatives. It is easy to show that a linear combination of terms cannot lead to a stable confinement for any finite range of coefficients.

For smooth ϕ fields, the last term represents a negative diffusion. If $\mu \leq \varepsilon$, where N is the number of terms in Eq. 2.2.2, the <u>total</u> diffusion is negative. However, the iteration Eq. 2.2.1 is still stable and converges for values of ε up to about 5μ, resulting in an effective negative diffusion coefficient in the long wavelength limit. Also, the discrete, converged solution can be given exactly in terms of sech functions.

The next step involves letting ϕ be the magnitude of vorticity and deriving an equation for the corresponding velocity correction that leads to Eq. 2.2.1 when the curl is taken (exactly in 2-D, or for a straight vortex in 3-D). This will result in a new formulation of Vorticity Confinement.

We simply define

$$\vec{q}^{\,n+1} = \vec{q}^{\,n} + \mu \nabla^2 \vec{q}^{\,n} + \varepsilon \vec{\nabla} \times \vec{w}^{\,n} \qquad 2.2.4$$

or, for $\vec{\nabla} \cdot q = 0$,

$$\vec{q}^{\,n+1} = \vec{q}^{\,n} - \vec{\nabla} \times \left(\mu \vec{\omega}^{\,n} - \varepsilon \vec{w}^{\,n} \right) \qquad 2.2.5$$

where

$$\vec{\omega}^{\,n} = \vec{\nabla} \times \vec{q}^{\,n} \qquad 2.2.6$$

and

$$\vec{w}^{\,n} = \frac{\vec{\omega}^{\,n}}{\left| \vec{\omega}^{\,n} \right|} \left[\frac{\sum_{l} \left(\left| \vec{\omega}_l^{\,n} \right| + \delta \right)^{-1}}{N} \right]^{-1} \qquad 2.2.7$$

where the sum is the same as in Eq. 2.2.2.

Results are presented in Fig.1 after 0, 8, and 100 iterations, for vorticity and velocity for a vortex in 2-D. Values used were $\mu = .2$, $\varepsilon = 0$ and $\varepsilon = 5\mu$. In this figure, the vorticity contour levels extend from about ¼ of the maximum initial value to the maximum so that a measure of the size of the confined region can be determined. We are currently investigating the new method for implementation in our codes. In addition, the use of the "Scalar Confinement" version, Eq. 2.2.1, is being used for flows where thin streams of passive scalars, such as contaminants, must be convected over long distances.

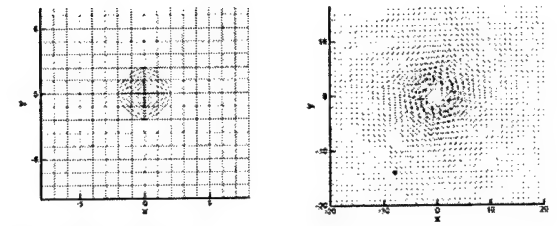

a) initial condition

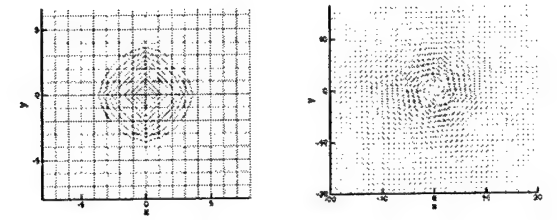

b)time steps = 8 $\varepsilon = 0$

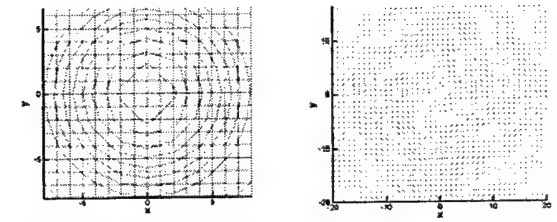

c)time steps = 100 $\varepsilon = 0$

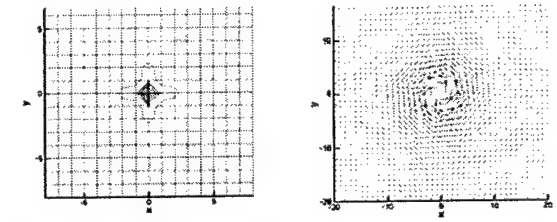

d) time steps = 8
$\varepsilon = 5\mu$

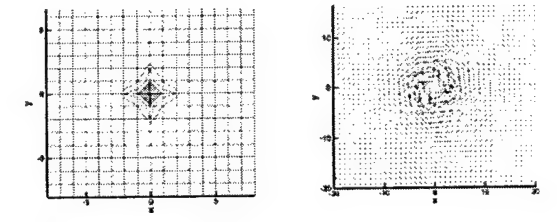

e) time steps = 100
$\varepsilon = 5\mu$

Figure.1 Vorticity contours and vector fields of velocity

3. Results

Three test cases are presented in this section. First, the effects of Vorticity Confinement on the wake structure of a 3-D circular and square cylinder are presented. The third example shows the application of Vorticity Confinement to a realistic flow simulation for a ship configuration.

3.1 3-D Cylinder

3.1a 3-D Circular Cylinder

Flow over a 3-D circular cylinder was calculated to assess the ability of Vorticity Confinement to accurately model the wake flow behind a blunt body. A long cylinder was "immersed" in a uniform $141\times101\times61$ Cartesian grid in the streamwise, normal and spanwise directions, respectively. Periodic conditions were imposed at the lateral boundaries. The diameter of the cylinder was 15 grid cells. The origin of the coordinate system used is located in the center of the cylinder, and all distances are non-dimensionalized by the diameter, shown in Fig. 2. Results of the computations were compared to the experimental results of Lourenco and Shih at a Reynolds number of about 3,900, described in Ref. [24]. The computational results were all averaged over the spanwise direction.

The diffusion coefficient μ was held constant for this study. The confinement coefficient, ε, was adjusted to impose different levels of confinement. This resulted in different levels of the intensity of the small vortical scales in the wake, and

approximately simulated different Reynolds numbers.

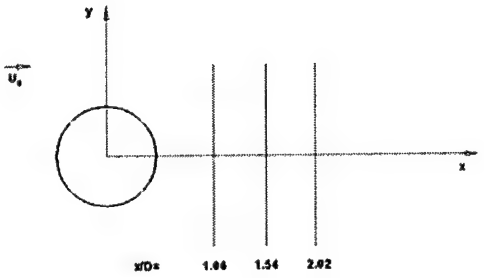

Figure 2. Measurement Positions For Circular Cylinder

Figure 3 depicts the mean streamwise velocities resulting from three values of the confinement coefficient. Figures a) and b) depict the result of two levels of confinement, where the flow is measured along lines which are normal to the cylinder axis and the mean stream, at three different locations in the wake of the cylinder shown in Fig. 2. For both values of ε the agreement can be seen to be very good, indicating that the effect of the confinement parameter is small over a range of values. Results from a case without confinement are depicted in Fig. 3c. Without confinement, the flow field is dominated by diffusive effects that are not counterbalanced by the anti-diffusive confinement term and approximates a steady, low Reynolds number flow.

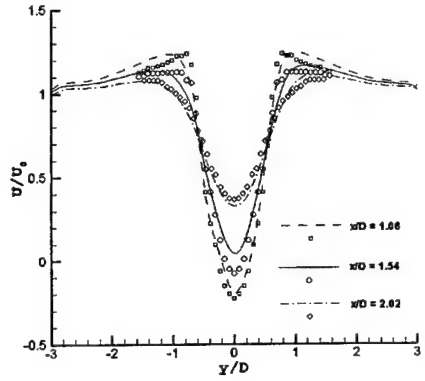

a) $\mu = 0.15$, $\varepsilon = 0.25$

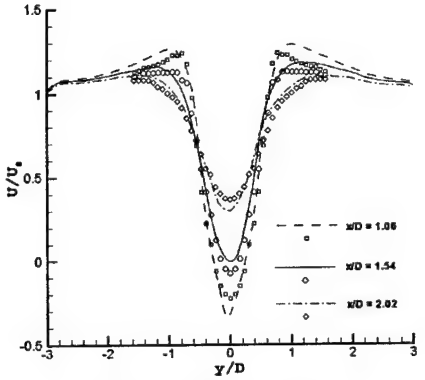

b) $\mu = 0.15$, $\varepsilon = 0.5$

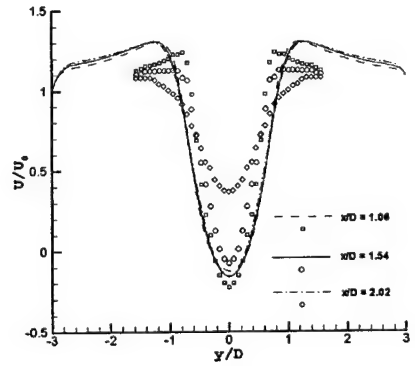

c) $\mu = 0.15$, $\varepsilon = 0.0$ (No Confinement)

Figure 3. Mean Streamwise Velocity Profiles. Symbols are experimental Data.

The ability of Vorticity Confinement to model a turbulent wake was assessed by computing the rms streamwise velocity fluctuations in the wake region. Comparisons of these

fluctuations with the experimental data were made along the same lines in the wake as for the mean velocity, for the same three values of ε. Fig. 4a (ε = 0.25) shows very good agreement. The effect of increasing confinement to 0.5 is depicted in Fig. 4b. In general, the effect of increased confinement is to thin the shear layer comprising the wake boundary, and to increase the fluctuation of the time-dependent flow from the mean flow. Fig. 4c depicts results without confinement. Without confinement, the flow can be seen to be steady and exhibits none of the fluctuations that would occur when confinement is used.

Figure 5 depicts isosurfaces of vorticity magnitude for the same three levels of confinement. The use of confinement results in chaotic flow patterns, as would be expected in three-dimensional turbulent flows. This does not occur in two-dimensional simulations, indicating that this chaotic behavior is not due to numerical instability created by the confinement. Increasing confinement increases the chaotic nature of the flow in 3-D and reduces the characteristic size of the vortical structures, analogous to what would be expected with an increase in Reynolds number. Clearly, the use of confinement allows small-scale time-dependent wake structures to be generated on extremely coarse grids with the small-scale structure captured over only 1~2 grid cells. Also, these small-scale structures serve as a viscous sink for turbulent energy, as in physical turbulence.

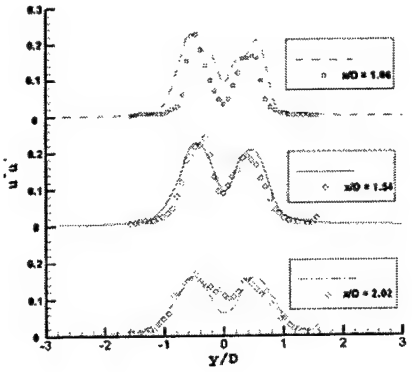

a) $\mu = 0.15$, $\varepsilon = 0.25$

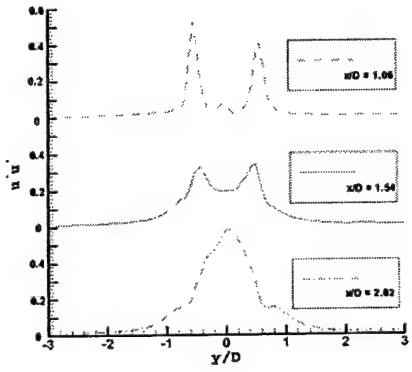

b) $\mu = 0.15$, $\varepsilon = 0.5$

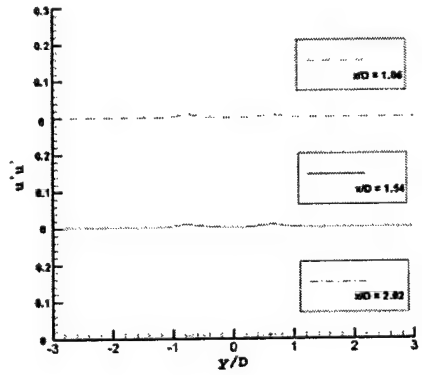

c) $\mu = 0.15$, $\varepsilon = 0.0$ (no confinement)

Figure 4. Streamwise Reynolds Stresses. Symbols Denote Experimental Data

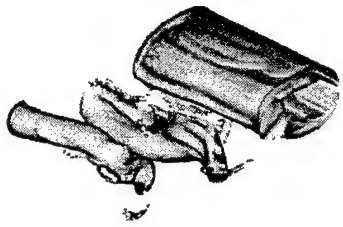

a) $\mu = 0.15$, $\varepsilon = 0.25$, Isosurface Level $= \pm 0.15$

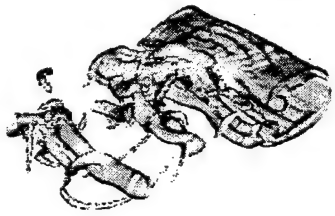

b) $\mu = 0.15$, $\varepsilon = 0.5$, Isosurface Level = ± 0.15

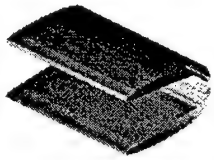

c) $\mu = 0.15$, $\varepsilon = 0.$, Isosurface Level = ± 0.15

Figure 5. Isosurfaces of Vorticity Magnitude

3.1b 3-D Square Cylinder

Flow over a square cylinder was also calculated. As in the circular case, the cylinder was "immersed" in a uniform $141 \times 101 \times 61$ Cartesian grid and periodic conditions imposed at the lateral boundaries. The diameter (length of each side) of the cylinder was also 15 grid cells. The same coordinate system was used as for the circular cylinder, as shown in Figure 6. Results of the computations were compared to the experimental results of Lyn et al. [25] at a Reynolds number of about 21,400. The computational results were all averaged over the spanwise direction.

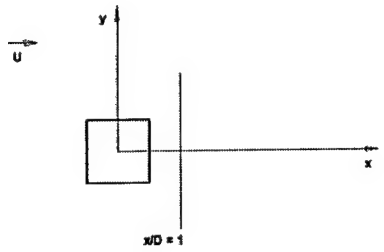

Figure 6: Measurement Positions For Square Cylinder

As in the circular cylinder case, the diffusion coefficient μ was also held constant at 0.15. The confinement coefficient, ε, was adjusted to impose different levels of confinement so as to approximate the effects of different Reynolds numbers.

Figure 7 depicts the comparison with experimental data of the time-averaged streamwise velocity along a streamwise line extending downstream from the middle of the leeward face of the cylinder. Results of two values of the confinement coefficient are plotted. Figure 8 shows the time-averaged

velocity along a line normal to the cylinder axis and the mean stream at x = 1. Symbols represent the experimental data. Our numerical results agree well with the experimental data.

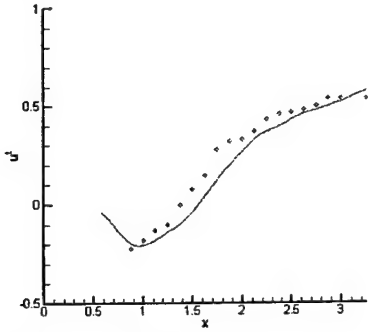

(a) $\varepsilon = 0.35$

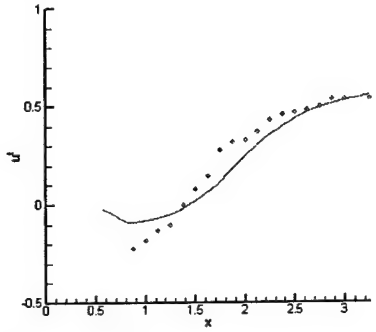

(b) $\varepsilon = 0.25$

Figure 7. Comparison of time-averaged streamwise velocity along a streamwise line. Symbols denote experimental data.

Comparisons of the computed turbulence level with the experimental results also show reasonably good agreement in Fig. 9a. The effect of decreasing confinement is shown in Fig. 9b. Comparing this case with the previous 3-D circular cylinder case, it is easy to see that a higher value of ε is required for better results. This is apparently because the Reynolds number has increased from about 3,900 in the 3-D circular cylinder case to roughly 21,400 in the present 3-D square cylinder case.

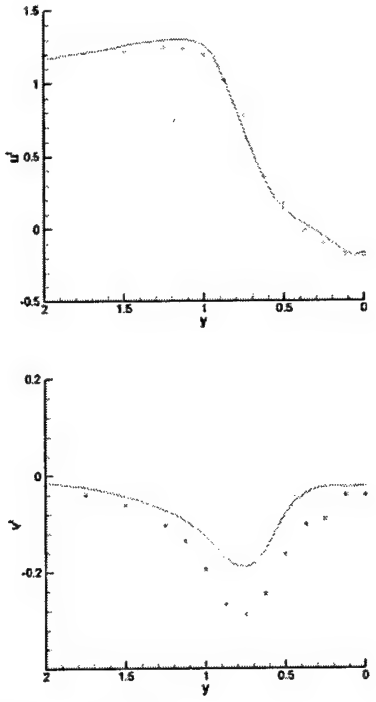

(a) $\varepsilon = 0.35$

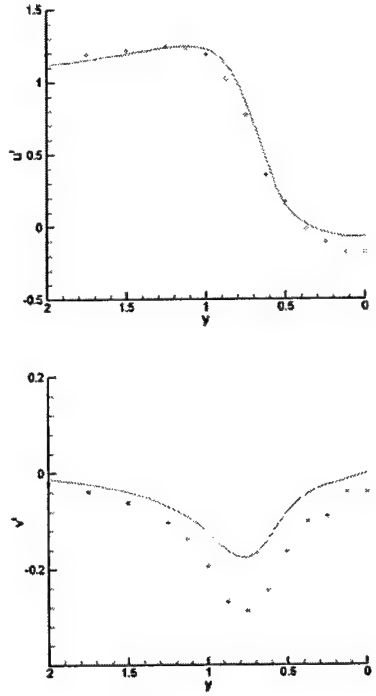

(b) $\varepsilon = 0.25$

Figure 8: Comparison of time-averaged velocity profiles at x = 1. Symbols are experimental data.

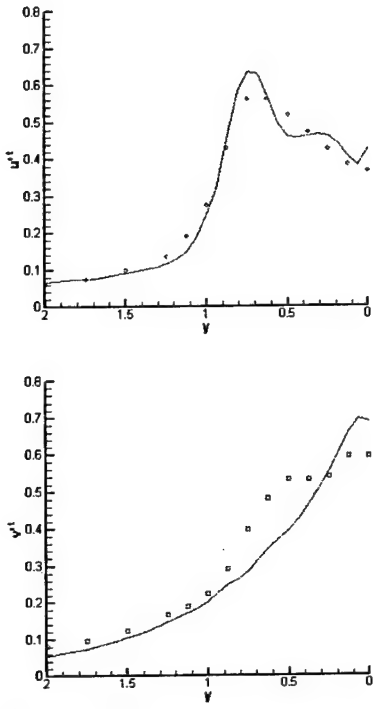

(a) $\varepsilon = 0.35$

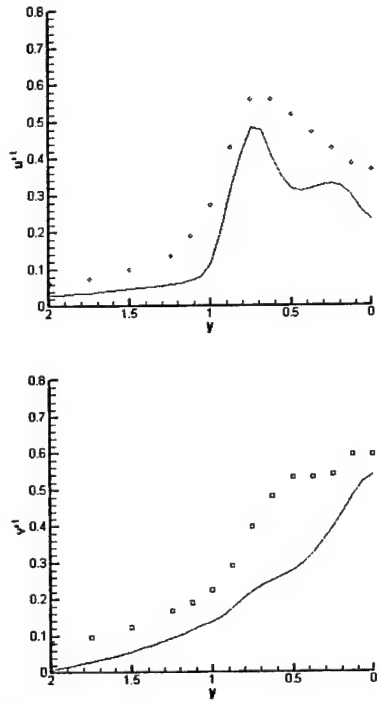

(b) $\varepsilon = 0.25$

Figure 9: Comparison of root mean square velocity fluctuation profiles at x = 1. Symbols are experimental data.

3.1c Synopsis of Cylinder Study

In subsequent studies, the correlation between ε and Reynolds number will be studied by comparisons between computation and experiment for other cases and a useful calibration of ε determined. Also, it should be emphasized that our agreement with experiment is closer than many much finer grid studies with much more complex LES pde models [26], each requiring a number of empirical coefficients. Just one coefficient is adjusted here, on a simple, coarse grid.

3.2 Ship Configuration

The present method of developing the operating limits for helicopters landing or taking off from ships is accomplished largely through flight tests, which are time-consuming, costly, and potentially dangerous. The ability to develop the operational limits using computational methods as an adjunct to present methods has the potential of significantly reducing cost, time, and risk. Figure 10 depicts the ship configuration used in this study, which has undergone wind tunnel testing by Caradonna [27].

The ship configuration is 80 units from bow to stern. The front of the bow is located at X=0; the Y=0 plane is perpendicular to the deck and is coincident with the deck midplane. The deck is 13 units wide, extending from Y=-6.5 to 6.5. The deck surface is located at Z=0, with positive Z upwards. The aerodynamic domain was modeled with two grids: a 401 x 121 x 74 grid extended from X=-50 to 150, Y=+/- 30, and Z=-6.5 to 30. Far-field boundary conditions were imposed on the surfaces

of this grid. A second grid was used to more highly resolve the forward deck region. The second grid (501 x 92 x 51) extended from X=-10 to 50, Y=-8 to 2.92, and Z=-2.5 to 3.5. Boundary conditions were imposed on the inner grid via interpolation. In addition, the outer grid obtained flow field information from the inner grid via interpolation at interior boundaries. As a result, two-way flow field communication was effected to obtain a globally consistent flow field. Velocities were measured on a plane (X=23.63) for a number of Z locations and were compared with computational results.

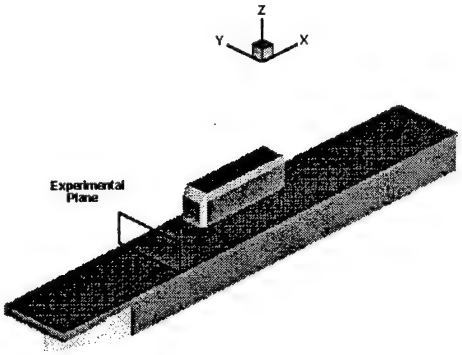

Figure 10. Helicopter Landing Ship

Figure 11 depicts vorticity isosurfaces over the ship deck for a wind aspect angle of 20°. Ship flow fields are often characterized by the development of a strong vortex at the windward edge of the deck that subsequently convects across the ship deck. The effect of field confinement is illustrated in a comparison between the isosurfaces of Figs. 11a and 11b. Without confinement (Fig. 11a), the vortex is greatly dissipated; with confinement (Fig. 11b), the deck vortex persists indefinitely over the deck surface. The view in Fig. 11 is looking down from above the deck with the bow at the bottom of the figure.

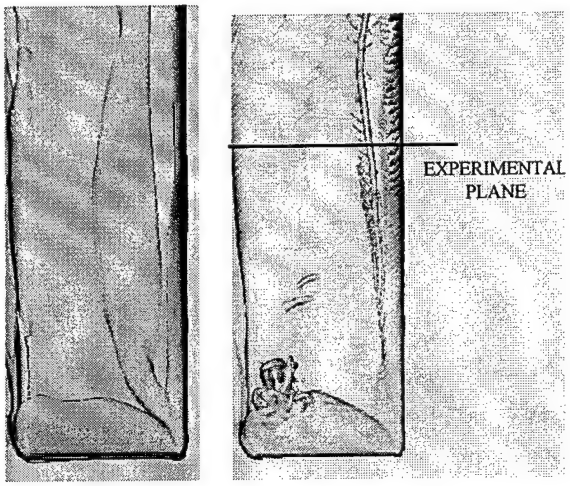

a) No Confinement b) With Confinement

Figure 11. Isosurface of Vorticity on Ship Deck

The computed vortex location is very close to the experimental location. These vortical structures are major features of the ship flow field, and would be difficult to resolve and maintain with conventional CFD methods without a much finer mesh. By contrast, the vortical structures are resolved and persist on a relatively coarse mesh with Vorticity Confinement. This is in accordance with physical expectations, in that the strength and structure of the vortices are maintained without significant dissipation. Quantitative results are presented in Fig. 12, which depicts velocity one unit above the deck at a constant height horizontal line that goes across the deck through the vortex center. The line is depicted (from above) in Fig. 11b as the "experimental plane". Additional information on the computation is given in Ref. [4].

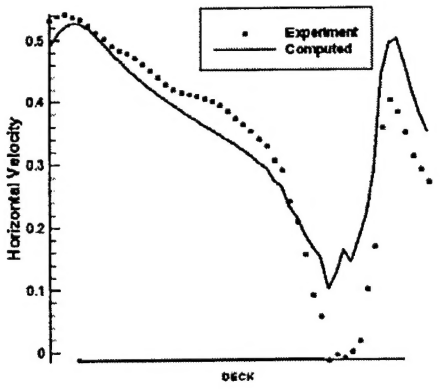

a) Horizontal Velocity

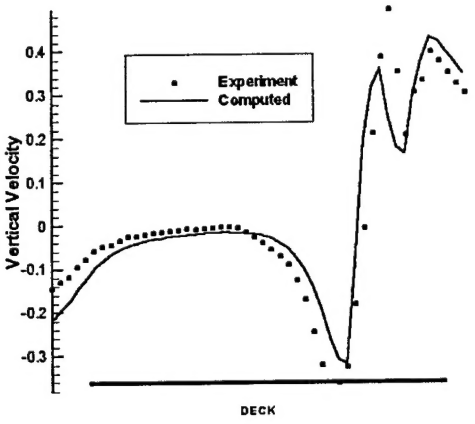

b) Vertical Velocity

Figure 12. Comparison of Experimental and Computed Velocity Over Deck, Z=1.0

4. Conclusions

Vorticity Confinement has been shown to provide an efficient, promising means of computing the turbulent wake behind a round and a square cylinder, on a very coarse mesh. Results were presented for the mean flow and the rms fluctuations, and the effects of different levels of confinement (and no confinement) were demonstrated. It appears that the ability to resolve scales down to 1~2 grid cells and absorb energy there suffices to quantitatively solve for the dynamics of the large scale eddies in the wake. Also, the method was shown to allow the emdedding of the surface in a uniform, coarse Cartesian grid without body-fitting, refinement, or complex logic near the surface.

It can be seen that the Vorticity Confinement results for the cylinder wakes, when compared to experiment, are comparable to conventional LES results. The difference is that the confinement solutions employ immersed boundaries with simple, coarse Cartesian grids, with only 16 grid cells across the cylinder diameter, and no complex LES turbulence pde models. As a result, no grid generation was required and the computations were very simple to set up and fast to run. Based on these results, it appears that Vorticity Confinement should be very useful for rapid engineering solutions for complex flows. Additional validation is being done for surface pressures and forces in these cases (beyond that already done) [5, 9]. Further, the functional dependence of our single constant, ε, on the Reynolds number is being calibrated by computing more cases.

Vorticity Confinement was also applied to a helicopter landing ship. In this case, the use of confinement was shown to be necessary, for the grid used, for the development of a deck vortex. This vortex is a major feature of ship flow fields at general wind aspect angles. The ship solution is of particular interest because, unlike the cylinder, the main vortical structures are not shed, but remain attached to the configuration. Although a very coarse mesh was able to

reproduce small-scale turbulent structure quite well with the cylinder, the ship required a more dense mesh near the corner of the bow to correctly predict the vortex generation. Similar results have been found in other cases. This is due to the interaction of the confinement terms with boundary conditions imposed by solid surfaces. This interaction is a subject of current research, as many structures (e.g., buildings) may exhibit bound vortices, and the ability to model these structures with coarse grids is of great importance.

Finally, a new, more elegant, fully conservative Vorticity Confinement formulation was presented with preliminary results with diffusion but without convection. This will be used in the future.

Acknowledgements

The authors would like to acknowledge the support of the Army Research Office and the Army Aeroflightdynamics Directorate for their support of this effect, and discussions with Dr. Frank Caradonna.

References

[1] VonNeumann, J., and Richtmyer, R.D., "A Method for the Numerical Calculation of Hydrodynamic Shocks", J. Appl. Phys., Vol. 21, No. 3, 1950.

[2] Lax, P.D., "Hyperbolic Systems of Conservation Laws II", Comm. Pure Appl. Math **10** (1957).

[3] Harten, A., "The Artificial Compression Method for Computation of Shocks and Contact Discontinuities III, Self-Adjusting Hybrid Schemes," *Mathematics of Computation*, Vol. 32, No. 142. April 1978.

[4] Fan, M., Dieta, W., Wenren, Y., and Steinhoff, J., "Computing Complex Flows on Coarse Grids Using Vorticity Confinement", AIAA-2002-0135.

[5] Steinhoff, J., Wenren, Y., Braun, C., Wang, L., and Fan, M. "Application of Vorticity Confinement to the Prediction of the Flow over Complex Bodies", pp. 197-226 in *Frontiers of Computational Fluid Dynamics 2002* (D.A. Caughey and M.M. Hafez eds.); World Scientific, (2002)

[6] Dietz,W., Fan, M., Steinhoff, J. and Wenren, J., "Application of Vorticity Confinement to the Prediction of the Flow over Complex Bodies", AIAA- 01-2642(2001).

[7] Wenren,Y., Fan, M., Dietz, W., Hu, G., Braun, C., Steinhoff, J., and Grossman, B., " Efficient Eulerian Computation of Realistic Rotorcraft Flows Using Vorticity Confinement", AIAA-01-0996 (2001).

[8] Hu, G., Grossman, B., and Steinhoff , J., "A Numerical Method for Vortex Confinement in Compressible Flow", AIAA-00-0281(2000).

[9] Wenren, Y., Steinhoff, J., Wang, L., Fan, M., and Xiao, M., "Application of Vorticity Confinement to the Prediction of the Flow over Complex Bodies," AIAA Paper No. 2000-2621, Fluids 2000, Denver, CO, June, 2000.

[10] Moulton, M., and Steinhoff, J., "A Technique for the Simulation of Stall

with Coarse-Grid CFD", AIAA-00-0277 (2000).

[11] Steinhoff, J., Wenren, Y. and Wang, L., "Efficient Computation of Separating High Reynolds Number Incompressible Flows Using Vorticity Confinement", AIAA-99-3316-CP (1999).

[12] Steinhoff, J., Puskas, E., Babu, S., Wenren, Y., and Underhill, D., "Computation of Thin Features Over Long Distances Using Solitary Waves," AIAA Proceedings, 13th Computational Fluid Dynamics Conference, July, 1997.

[13] Steinhoff, J., and Raviprakash, G., "Navier-Stokes Computation of Blade-Vortex Interaction Using Vorticity Confinement", AIAA-95-0161.

[14] Steinhoff, J. and Underhill, D., "Modification of the Euler Equations for Vorticity Confinement Application to the Computation of Interacting Vortex Rings," *Physics of Fluids*, 6, 1994.

[15] Steinhoff, J., "Vorticity Confinement: A New Technique for Computing Vortex Dominated Flows," In D.A. Caughey and M.M. Hafez, editors, *Frontiers of Computational Fluid Dynamics*. John Wiley & Sons, 1994.

[16] Steinhoff, J., Wenren, Y., Mersch, T., and Senge, H., "Computational Vorticity Capturing: Application to Helicopter Rotor Flow", AIAA-92 (Reno) (1992).

[17] Steinhoff, J., Wang, Clin, Underhill, D., Mersch, T., and Wenren, Y., "Computational Vorticity Confinement: A Non-Diffusive Eulerian Method for Vortex-Dominated Flows," UTSI preprint, 1992.

[18] Lohner, R., and Yang, C., "Vorticity Confinement on Unstructured Grids", AIAA-2002-0137.

[19] Murayama, M., Nakahashi, K. and Obayashi, S., "Numerical Simulation of Vortical Flows Using Vorticity Confinement Coupled with Unstructured Grid", AIAA-01-0606 (2001).

[20] Grossman, B., and Hu, G., "The Computation of Vortex Dominated Flows Using Compressible Vorticity Confinement Methods", AIAA-2002-0136.

[21] Fedkiw, R., Stan, J. and Jensen, H.W., "Visual Simulation of Smoke", pp.15-22 in Proc. SIGGRAPH 2001, Los Angeles, CA (2001).

[22] Caradonna, F., "Developments and Challenges in Rotorcraft Aerodynamics", AIAA-00-0109 (2000).

[23] Steinhoff, J., Fan, M. and Wang, L., "Convection of Concentrated Vortices and Passive Scalars as Solitary Waves", UTSI preprint, 2002.

[24] Ma, X., Karamanos, G., and Karniadakis, G., "Dynamics and Low-Dimensionality of a Turbulent Near Wake," *J. Fluid Mech.*, **410**, pp. 29-65, 2000.

[25] Lyn, D.A., Einav, S., Rodi, W., and Park, J.H., "A Laser-Doppler Velocimetry Study of Ensemble-Averaged Characteristics of the Turbulent Near Wake of a Square Cylinder ", *J. Fluid Mech.*, **304**, pp. 285-319, 1995.

[26] Rodi, W., "Large-Eddy Simulation and Statistical Turbulence Models: Complementary Approaches", *New Tools In Turbulence Modelling*, Eds. Metais, O. and Ferziger, J., Springer-Verlag 1997.

[27] Caradonna, F., Wind Tunnel Measurements, Army Aeroflight Dynamics Group, Moffett Field, CA, Private Communication, Feb. 2001.